A GENERALISED OSCILLATOR STRENGTH STUDY OF ATOMIC HYDROGEN

by

HASAN BOLOURI

A thesis submitted for the degree of

Master of Philosophy

Department of Physics,

University of Southampton,

February, 1978

PREFACE

This thesis is based on the experiment, carried out at one of the Atomic Collision laboratories of the University of Southampton between October, 1975 to 1977. I would like to take this opportunity to thank all of the many people who have assisted me during the course of this work.

I am grateful to Dr. Kevin Ross, my supervisor, for introducing me to this subject and giving helpful guidance throughout this research. Thanks are also due to Dr. Mel White for many useful and illuminating discussions. The co-operation of my colleagues, Mr. G. Kavei and Mr. D. Rassi is also appreciated.

Last, but not least, I would like to express my sincere thanks to my family, whose ceaseless moral and financial support was a major factor towards completion of this project. They deserve my warmest thanks and gratitude.

H.B.

CONTENTS

ABSTRACT

Faculty of Science

Physics

Master of Philosophy

A GENERALISED OSCILLATOR STRENGTH STUDY OF ATOMIC HYDROGEN

Hasan Bolouri

The collision cross section of atomic hydrogen for excitation by electron impact has been studied. Generalised Oscillator Strength data are presented for incident electron energies of 136, 200 and 300 eV.

The electron spectrometer consisted of an electron gun to produce the incident beam, and an hemispherical electrostatic velocity analyser and associated electron optics to detect the scattered current. The spectrometer was capable of producing an incident electron beam with energies in the range 50 to 500 eV, with detection of energy losses of 0 to 50 eV in the scattered beam. To facilitate the study of angular dependence on Generalised Oscillator Strength, electron scattering could be detected in the range -7 to +20 degrees. Atomic hydrogen was produced in a flowing afterglow from a microwave cavity discharge.

The Generalised Oscillator Strengths derived from the cross-section measurements are compared with theoretical Born approximation calculations, close-coupling calculations, and also with the experimental results of Williams et al (1975); the latter results differ from the present work by 31% at 300 eV, 30% at 200 eV and 41% at 136 eV. Within the experimental error, no difference is observed between the present results and the results, predicted by theory.

In addition, an investigation to find the ideal conditions for operating the electron gun led to a series of experiment whose results are presented in Chapter 4. This study confirmed some of the earlier work on the subject.

CHAPTER 1

INTRODUCTION

1.1 Electron-Atom Collisions

Atomic physics is a relatively young science, having been developed mostly in this century. However, the idea that matter is built up of atoms is a very old one. Perhaps the Greek philosopher, Democritus (460-370 B.C.) for example, was one of the earliest who theorized that matter consists of particles.

Spectroscopy is essentially the determination of energy levels of atoms, molecules and nuclei. The atoms in this process need to be excited in one of the several possible ways of which excitation by impact with electron, the elementary quantum of electricity, is the subject of the present work.

The theory of electron-atom collision has been developed very intensively in the last few years. Electron energy-loss spectroscopy of gases and vapours has been demonstrated to be a powerful spectroscopic technique as well as enabling studies of the differential inelastic collision cross-section to be made.

Early in the century, Bohr (1913) investigated the velocity of moving particles on passing through matter, and the first experimentation on detailed features of inelastic collision dates back to the famous works of Frank and Hertz (1919) who measured energy losses of electrons passing through gases and thereby demonstrated the existence of discrete excitation energies in atoms. In 1929, the energy loss spectrum of nitrogen was reported by Harnwell. Introduction of the first electrostatic analyser by Hughes and Rojansky in 1929 improved the resolution of electron energy loss investigations during 1930's. Bullard and Massey (1931) studied angular distribution of electron-argon collision. In 1930 Bethe established a quantum mechanical theory for electron collisions, based on the Born approximation and thereby derived a number of important results concerning collision cross sections and

the stopping power for fast particles.

Most of the early research was directed towards establishing that electron energy loss spectra revealed similar features to those of photo-absorption. Womer (1934) attempted to correlate the relative intensities of transitions in the energy loss spectra for different electron incident energies. Whiddington and Co-workers (1934) investigated inelastic electron scattering in helium, neon and argon. The development of new types of electron spectrographs with resolution of 1 in 10^5 at 50 KeV, by Mollenstedt (1949) and Blackstock et al. (1955) led to the intensive investigations of the characteristic energy losses in solids and the development of the plasma oscillation theory. Similar analysers were applied to studies of atomic gases by Dietrich (1956) and, also by Geiger (1964).

The experiments of 1930 were limited by serious experimental difficulties in producing large and detectable signal strength. Simpson (1964), for the first time, suggested using a second analyser for producing a monochromized incident electron beam. Inspiring works of Lassettre and Co-workers during 1960's, characterised by remarkably improved resolution both in electron energy and in beam callimation, provided a basis for more technical investigations in energy loss spectroscopy. Bromberg (1969) measured absolute differential cross section of elastically scattered electrons in different gases. His work established a new and superior normalisation technique for inelastic collision cross-section measurements. Low energy electron-atom collisions have been studied by Doering et al. (1967), Kupperman et al. (1968) and Trajmar et al. (1971) and have established a valuable basis for the understanding of exchange phenomena. Present day atomic collision physics is truly indebted to the theoretical works of Mott & Massey (1949). Electron energy loss spectroscopy is also now being used in a coincidence technique for identifying the decaying states of auto-ionizing ejected electrons

excited by electron impact (Dillon & Lassettre (1975), Van der Wiel et al. (1973) and El-Sherbini (1972).

The experimental determination of absolute collision cross-section would be greatly simplified if all cross sections could be measured relative to some standard cross sections which are known accurately. Since atomic helium is a readily available atom which is easy to use experimentally, and since it is also relatively simple to treat theoretically, it has been suggested that the electron excitation cross section for the $1^1S \rightarrow 2^1p$ transition in helium would be a suitable standard cross section (Lassettre and Jones, 1964). Because it is necessary to use approximate wave functions for both the initial and final states of the transition, the Born approximation expression for the cross section cannot be evaluated exactly and although extensive calculations have been carried out (Lassettre and Jones, 1964 and Mott and Massey, 1965), it is difficult to estimate the accuracy of the calculated cross-sections.

Theoretical collision cross section calculations are still seriously limited by wavefunction calculations and consequently the only stringent test of collision theories are for the cases of the simple helium and hydrogen atoms. Theoretical calculations on $1^1S \rightarrow 2^1p$ transition in helium have been made by Massey and Mohr (1931), using the Born approximation and screening constant wavefunctions for helium. Rothenstein (1954) extended the calculations to include the second Born approximation. For the ground state of helium he used the Eckart (1930) function. Rothenstein calculated cross-sections for incident electron energies below 150 volts. The above theoretical works suggest that the Born approximation provides a satisfactory method for this transition at kinetic energies of several hundred volts. This conclusion was later confirmed by the fact that the cross-section formula, obtained by Massey and Mohr, agree fairly well with the experimental measurement of cross section at a kinetic energy of 200 eV (Massey, 1956). Further calculations, employing more accurate functions, were made by

Lassettre et al. (1964). Helium-electron collision cross sections, as a function of scattering angle, were experimentally studied and four transitions ($1^1S \rightarrow 2^1p$, $1^1S \rightarrow 2^1S$, $1^1S \rightarrow 3^1p$ and $1^1S \rightarrow 2^1p$) at incident energy of 511 volts were observed.

Accurate measurement of differential cross section of electron-helium collision were determined by Bromberg (1969) who also studied other gases. The scattering of electron by helium was extensively studied by Dillon et al. (1975) at kinetic energies of 200 to 700 volts. The $1^1S \rightarrow 2^1S$ and $1^1S \rightarrow 2^1p$ transitions at scattering angles within the range $7.5 - 35^o$ were investigated and generalised oscillator strengths were calculated from the data for both the transitions. Comparison of results with the Born approximation calculations of Kim and Inokuti (1968) showed a deviation from the Born approximation, mostly below 300 eV incident energy.

Theoretical calculations for electron-hydrogen atom collisions have been carried out sporadically since 1927 but enthusiasm for this work was tempered at first by the lack of available experimental information about the different cross-sections. This was not surprising, due to the difficulty of making quantative measurements with atomic hydrogen. Since the 1940's the development of variation methods for dealing with collision problems (see Mott and Massey, 1949, for example) directed attentions again to the collision of electrons with hydrogen atoms for which they could be more fully exploited. The study of atomic hydrogen has received much more attention from the theoretical physicists than any other element, as was said before, due to the relative simplicity of the system and the availability of accurate atomic wavefunction.

It should be known, however, that even for this case, still no exact solution for the problem of the excitation of the two lowest states of atomic hydrogen, 2S and 2p states, has been obtained. The only method by which one can assess the accuracy of the various approximations which have

been employed, is by comparing them with each other and with the available experimental data.

1.2 Generalized Oscillator Strength

The generalised oscillator strength of an atom or molecule is an important property representing the response of the system to sudden transfer of momentum to its electrons. In particular, it constitutes the essential part of the differential cross section for inelastic scattering of sufficiently fast charged particles. The well known prescription for its evaluation requires the wave functions for the initial and final states of the system, which are in general known only approximately, often only crudely, except for the case of atomic hydrogen. This deficiency has hampered the application of the Bethe theory to its full extent, even to the relatively simple case of the helium atom. For transitions from the ground state to excited states, many calculations are found in the literature but the approximate nature of the wavefunctions used does not always convince one of the reliability of the results, which appear in many cases, quite sensitive to the choice of the wave functions. Current experiments on inelastic scattering of electron beams with high energy resolution and good collimation are providing data of remarkable quality (Lassettre and co-workers, Simpson and co-workers, for example).

The generalised oscillator strength was introduced by Bethe in 1930 and was used in his stopping power theory. Massey and Mohr (1931) calculated the inelastic cross section of the singlet and triplet terms of helium and and hydrogen spectrum. The Bethe theory of the energy loss of fast charged particles was extended for treating the stopping contribution of K-shell electrons (Walske, 1952), and L-shell electrons (Walske, 1956). Cross-section calculations were carried out by Bates and Damgaard (1949), Gree et al. (1951), and Seaton (1951).

Altshuler (1952) calculated the cross sections for three transitions ($1^1S \rightarrow 2^1p$, $1^1S \rightarrow 3^1p$ and $1^1S \rightarrow 2^1S$) of helium in two different formulations.

These calculations formed the theoretical basis for the comparison made by Lassettre et al., (1958), who experimentally measured the Generalised Oscillator Strength for the above transitions. The inelastic cross section of electron-hydrogen scattering for transition 1S → 2S and 1S → 2p was calculated by Burke et al.(1963). Omidvar (1965) measured the atomic form factor, and consequently, the Generalised Oscillator Strength of the hydrogen atom in excitation by electron impact.

Investigating different transitions in helium has been the subject of many studies during 1960's. For example, the Generalised Oscillator Strength of helium from its ground state to excited states n = 2^1p, 3^1p 2^1S and 3^1S were computed by Kim and Inokuti (1968). Lassettre's electron scattering experiments provided the first extensive experimental measurements of atomic and molecular Generalised Oscillator Strength. These experimental Generalised Oscillator Strength measurements have been applied by Green and Peek (1968) to certain molecular scattering problems. Rau and Fano (1967) have obtained asymptotic properties of Generalised Oscillator Strength. Inokuti and Kim (1968) and Oldham (1968) have made accurate calculations of Generalised Oscillator Strength for a limited number of discrete excitations in helium.

Bell, Kingston and Kennedy (1968) have made similar calculations for a wide range of discrete excitations with a less accurate ground-state wave-function. Bell and Kingston (1969) calculated cross sections for proton and electron ionisation for helium.

Minima in atomic continuum Generalised Oscillator Strength were studied by Manson (1970) and showed that at increased energy loss they occur at larger momentum transfer.

Numerous publications on the excitation of atoms report the integrated cross-sections, thus bypassing a discussion of the differential cross-section, or the Generalised Oscillator Strength. In as much as the differential cross-section provides a far more stringent test of both theory and experiment, it is hoped that future investigators will publish differential cross-section

data in as much detail as possible.

The apparatus on which the present investigation was performed, was basically the same apparatus as had previously been used for the study of high resolution electron energy loss in atomic nitrogen and hydrogen (White, 1976). Initially, the signal strength attainable from the apparatus appeared inadequate to enable us to study the generalised oscillator strength. Also the dissociation ratio $(\frac{H}{H_2})$ was so low that electron atomic scattering could only be observed at zero degrees.

This thesis describes the measures taken to increase the signal strength and the generalised oscillator strength results obtained for atomic hydrogen.

CHAPTER 2

THEORY

2.1 Born Approximation

To explain the Born approximation, we first consider the case of elastic scattering and then extend it to the case of inelastic scattering. This procedure is used since the elastic Born approximation provides a simpler basic understanding of the scattering theory.

2.1.1 Born Approximation in Elastic Scattering

The problem of the potential scattering of a particle of mass m_1 by a target of mass m_2 may be reduced to the problem of the scattering of a particle with reduced mass μ ($\mu = \frac{m_1 m_2}{m_1+m_2}$) in a potential v(r). The Schrödinger equation is:

$$(\nabla^2 + k^2)\ \psi(r) = \frac{2\mu V(r)}{\hbar^2}\ \psi(r) \tag{2.1}$$

where

$$k^2 = \frac{2\mu E}{\hbar^2} \tag{2.2}$$

and $\psi(r)$ is the particle wavefunction (see for example, Davydov, 1965).

The scattering space may be divided into two regions: the region within the range of the force, and a region in which particles are free moving. Particles in the free moving region may be represented by a plane wave.

$$\phi_{a(r)} = \exp i\ (K_a.r) \tag{2.3}$$

$$(Ka^2 = K^2)$$

By using Green function, the asymptotic form of $\psi a(r)$ is obtained:

$$\psi_a(r) = \exp i\ (K_a.r) + A_{ba}\ \frac{e^{ikr}}{r} \tag{2.4}$$

which is simply the incident wave plus the scattered wave and therefore, A_{ba} is the scattering amplitude, given by the formula:

$$A_{ba} = -\ \frac{\mu}{2\pi\hbar^2}\ \langle\phi_b|V|\psi_a\rangle \tag{2.5}$$

Assuming the interaction energy V(r) to be a small perturbation, we can solve

(2.4) by the method of successive approximations. The result is:

$$\psi_{a(r)} = \phi_a(r) - \frac{\mu}{2\pi\hbar^2}\int \frac{e^{ik|r-r'|}}{|r-r'|} V(r')\ \phi_a(r')d_3r' + \ldots \quad (2.6)$$

So, the scattering amplitude will have the following property:

$$A_{ba} = \frac{-\mu}{2\pi\hbar^2} <\phi_b|V|\phi_a> + (\frac{\mu}{2\pi\hbar^2})^2\int \phi_b^*(r) \frac{e^{ik|r-r'|}}{|r-r'|} V(r)V(r')\phi_a(r')d^3rd^3r'+\ldots \quad (2.7)$$

Depending on which terms we retain in this series, we obtain different orders of the Born approximation.

For the first Born approximation which corresponds to the first of the successive approximation in which

$$\psi_a(r) = \exp i\ (k_a.r)$$

is used as the first estimate of $\psi_a(r)$, the result is:

$$A_{ba} = -\frac{\mu}{2\pi\hbar^2} <\phi_b|V|\phi_a> \quad (2.8)$$

The factor of particular interest in collision theory is the scattering cross-section ($\frac{d\sigma}{d\Omega}$) which determines the number of particles scattered at angle θ per unit time per unit solid angle:

$$\frac{d\sigma}{d\Omega} = (\frac{\mu}{2\pi\hbar^2})^2 |<\phi_b|V|\phi_a>|^2 \quad (2.9)$$

2.2 The Collision of Electrons with Hydrogen Atoms (Inelastic Scattering)

Generally, in an elastic collision no energy exchange takes place between the internal motion of the atom and the electron . Only a fraction of order $\frac{m}{M}$ (mass of electron to that of the atom), of the initial kinetic energy of the electron is lost. In inelastic collisions,which are the subject of interest in the present work, some kinetic energy is lost by the electron in exciting internal motion in the atom.

The wave equation for the system of incident electron and hydrogen atom is (see Mott and Massey, 1965):

$$\frac{\hbar^2}{2m}\left(\nabla_1^2 + \nabla_2^2\right) + E + \left(\frac{\varepsilon^2}{r_1} + \frac{\varepsilon^2}{r_2} - \frac{\varepsilon^2}{r_{12}}\right)\psi = 0 \qquad (2.10)$$

where

$$\frac{\varepsilon^2}{r_1} + \frac{\varepsilon^2}{r_2} - \frac{\varepsilon^2}{r_{12}} = V \qquad (2.11)$$

and ψ is the wavefunction. In this formula, the incident electron is distinguished by the suffix 1 and the atomic electron by the suffix 2. The energy E is the sum of the energy E_o of the atomic electron in its ground state and of the kinetic energy $\frac{1}{2}mv^2$ of the incident electron. The motion of the proton in the collision is small compared with that of the electron and is neglected.

$\psi(r_1,r_2)$ may be expanded in terms of the proper wavefunction ψ_n of the hydrogen atom :

$$\psi(r_1,r_2) = \left(\sum_n + \int\right) \psi_n(r_2)F_n(r_1) \qquad (2.12)$$

Substituting (2.12) into (2.10), we obtain:

$$\left(\Sigma_n + \int\right) \psi_n(r_2) \left\{\frac{\hbar^2}{2m}\nabla^2 + E - E_n\right\} F_n(r_1) = \left(\frac{\varepsilon^2}{r_{12}} - \frac{\varepsilon^2}{r_1}\right)\psi(r_1,r_2) \qquad (2.13)$$

Multiplying both sides of (2.13) by $\psi_n^*(r_2)$ and integrating over the co-ordinate space of the atomic electron results:

$$\left\{\frac{\hbar^2}{2m}\nabla^2 + E - E_n\right\} F_n(r_1) = \int\left(\frac{\varepsilon^2}{r_{12}} - \frac{\varepsilon^2}{r_1}\right)\psi(r_1,r_2)\psi_n^*(r_2)d\tau_2 \qquad (2.14)$$

For large r_1 the right hand side vanishes, and F_n satisfies the following equation:

$$\left\{\nabla^2 + \frac{2m}{\hbar^2}(E - E_n)\right\} F_n = 0 \qquad (2.15)$$

which is the wavefunction for a free particle of energy $E - E_n$.

Since the conditions of the problem require the electron to be incident on an atom in its normal state, the function $F_o(r_1)$ must represent the sum of an incident and scattered wave; thus F_o must have the asymptotic form:

$$F_o \sim e^{ik_o z} + r^{-1} e^{ik_o r} f_o(\theta,\phi) \qquad (2.16)$$

the function F_n must represent scattered waves only, and so have asymptotic form:

$$F_n \sim r^{-1} e^{ik_n r} f_n(\theta,\phi) \tag{2.17}$$

Equation (2.14) represents the exact solution to the scattering problem but can not be solved exactly. However, for a small scattering potential (v), ψ may be approximated to take the following form:

$$\psi = \exp\,(i.K_o.n_o.r_1)\psi_o\,(r_2) \tag{2.18}$$

this is simply the product of the incoming plane wave and the unperturbed atomic wavefunction in the ground state. This zero-order approximation assumes small interaction only. Substituting (2.18) in (2.11) produces the first Born approximation:

$$\frac{\partial I_{on}}{\partial \omega} = \frac{4\pi^2 m^2}{h^4} \frac{\bar{K}_n}{K_o} \left[\iint V_A \exp\left[i(\bar{K}_o.\bar{n}_o - \bar{K}_n.\bar{n}_n).R \right] \psi_o \psi_n^*(\partial \bar{R}) \partial \tau \right]^2 \tag{2.19}$$

and higher orders are obtained by successive iterations (see Moiseiwitsch and Smith, 1968). In this formula, $\frac{\partial I_{on}}{\partial \omega}$ is the cross-section for scattering at angle θ into unit solid angle from state o to state n. Suffixes o and n are employed to indicate the electron situation before and after scattering. $\bar{n}_o$ and $\bar{n}_n$ are unit vectors along the directions of incident and scattered beam respectively. V_A is the interaction potential, $\bar{R}$ is the position vector of the colliding electron and $\partial \bar{R}$ is the colliding electron volume element.

A transformation of equation (2.19), first used by Bethe (1930), reduces it to a form more useful in application. This transformation, which is also described in detail by Mott and Massey (1949), results in the following expression:

$$\frac{\partial \sigma_{on}}{\partial \omega} = \frac{4P_n}{P_o} \frac{\varepsilon_n \varepsilon_n^*}{(\Delta P)^4} \tag{2.20}$$

and is called the Bethe-Born differential cross-section for inelastic scattering, where:

$$\epsilon_n(\Delta P) = \sum_s \int \exp\,(i.\bar{\Delta P}.\bar{r}_s)\psi_o\psi_n^* \,\partial\tau \qquad (2.21)$$

For a detailed discussion of inelastic scattering, see Mott and Massey (1949).

2.2.1 Validity of the Born Approximation

In electron-atom collision theory it is of importance to know the incident electron energy range in which the first Born approximation is valid. The Generalised Oscillator Strength (introduced in the following section) is also based on this approximation and therefore depends on its validity.

A necessary, but not sufficient condition for validity of the Born approximation is that the incident energy of the electron must be high compared with the excitation energy, i.e.:

$$E_o >> W \tag{2.22}$$

In order to satisfy the small perturbation, assumed in the calculation, in terms of the square of the momentum, (2.22) may be expressed as:

$$\frac{P_1^2}{2} >> W \tag{2.23}$$

Here, E_1 and W are the incident and excitation energies of the electrons respectively, and P_1 is the momentum of the incident electrons. If P_2 is the momentum of the scattered electrons, (see section 2.5)

$$W = \tfrac{1}{2}P_1^2 - \tfrac{1}{2}P_2^2 \qquad \text{or} \qquad \tfrac{1}{2}P_2^2 = \tfrac{1}{2}P_1^2 - W$$

Regarding (2.23), a necessary condition for the validity of the Born approximation is obtained as:

$$P_2 \simeq P_1 \tag{2.24}$$

i.e.: small momentum transfer ($\bar{\Delta}P$).

Detailed discussion on this subject, on the electron excitation of the 2S and 2P states of atomic hydrogen, using a simplification of the second Born approximation without exchange by Holt and Moiseivitsch (1968), shows that if the incident electron energy is about five times the excitation energy, then the first Born approximation overestimates the 1S → 2S and 1S → 2P cross-sections by about 25% and 10% respectively. The convergence of the Born approximation has also been considered by Mott & Massey (1965), but in general, it is not possible to specify the range of validity of the first

Born approximation for a particular transition. However, in general, it should be remembered that the Born approximation is a high incident energy, small momentum transfer theory.

2.3 Generalised Oscillator Strength

The concept of Generalised Oscillator Strength was first introduced by Bethe (1930) who emphasised its usefulness in applications where the Born approximation is used. Consider an inelastic collision between an electron and an atom (or molecule), where excitation occurs to an upper quantum state whose energy exceeds that of the ground state by amount W_n. If the momentum vectors for the incident and scattered electrons are called P_1 and P_2, then the quantity which is known as the Generalised Oscillator Strength is defined in atomic units as following:

$$f_{on}(\bar{\Delta P}) = \frac{2W_n}{(\Delta P)^2} \left| \varepsilon_n(\bar{\Delta P}) \right|^2 \qquad (2.25)$$

ΔP is the difference in electron momentum vector before and after scattering:

$$(\Delta P)^2 = P_1^2 + P_2^2 - 2P_1P_2 \cos\theta \qquad (2.26)$$

the Generalised Oscillator Strength is not a directly observable quantity, but an experimental Generalised Oscillator Strength (f') derived from the following equation can be determined:

$$f'_{on}(\bar{\Delta P}, E_o) = \frac{W_n}{2} (\Delta P)^2 \frac{P_o}{P_n} \frac{\partial \sigma_{on}}{\partial \omega} \qquad (2.27)$$

and $$f'_{on}(\bar{\Delta P}, E_o) = f_{on}(\Delta P)$$

only if the Born approximation is valid for the interpretation of $\frac{\partial \sigma}{\partial \omega}$.

Another form of $f_{on}(\Delta P)$ is obtained by expanding (2.20) and (2.25) for $(\Delta P)^2 << 1$ as follows:

$$f_{on}(\Delta P) = 2W_n \left[\varepsilon_1^2 + (\varepsilon_2^2 - 2\varepsilon_1\varepsilon_3) \Delta P^2 + \ldots \right] \qquad (2.28)$$

this expression for $f_{on}(\Delta P)$ is considered in detail in section (2.4).

2.3.1. Properties of Generalised Oscillator Strength

(1) Equation (2.28) shows that the Generalised Oscillator Strength approaches to the optical Oscillator Strength as ΔP approaches zero:

$$f_{on}\ \underset{(\Delta P)^2 \to 0}{(\Delta P)^2 \to} f_{on}(0) \tag{2.29}$$

therefore, the optical oscillator strength may be used to normalise electron-atom scattering cross section or Generalised Oscillator Strength. See for example Newell and Ross (1971).

(2) Sum Rules: the average of the energy transfer to the atom over all modes of internal excitation for a given $(\Delta P)^2$ must be the same as that given to Z free electrons:

$$\sum_n \frac{2W_n}{(\Delta P)^2}\ \varepsilon_n\ (\bar{\Delta P}) = Z \tag{2.30}$$

or

$$\sum_n f_{on}\ (\bar{\Delta P}) = Z \tag{2.31}$$

This also provides a useful method of normalisation. See for example, Hertel and Ross (1968).

(3) The Generalised Oscillator Strength for a given transition is a function of only one variable, involving the incident and scattered electron (i.e. the quantity ΔP). So a plot of Generalised Oscillator Strength against $(\Delta P)^2$ is expected to be independent of incident electron energy. This provides a necessary, but not sufficient test of the validity of the Born approximation. See for example Dillon and Lassettre (1975).

2.4 Optically Allowed and Forbidden Transitions

Transitions can be divided into two categories: those which obey the selection rules for electric dipole transitions (optically allowed) and transitions which do not obey the electric dipole selection rules (optically forbidden). For high incident energies and zero scattering angle, $(\Delta P)^2$ tends to zero. In the case of an optically allowed transition, $\varepsilon_1 \neq o$ and from equation (2.28), when $(\Delta P)^2$ is negligibly small, all other terms vanish. Thus as $(\Delta P)^2 \to o$, then

$$f_{on}(\Delta P) = 2W_n \varepsilon_1^2 = f_{on}(0) \tag{2.32}$$

$f_{on}(0)$ is the optical oscillator strength.

This point may be used for normalisation by extrapolating experimental data back to $(\Delta P)^2 = o$.

In the case of forbidden transition ε_1 vanishes. If $\varepsilon_2 \neq o$ and we neglect higher orders of (ΔP), we obtain from (2.28):

$$\varepsilon_1 = 0 \qquad f_{on}(\Delta P) = 2W_n \varepsilon_2^2 (\Delta P)^2 \tag{2.33}$$

To distingusih between these two different types of transitions, using electron energy loss techniques, one can measure the Generalised Oscillator Strength for each of them in the limiting $(\Delta P)^2 \to o$.

For an allowed transition

$$\lim_{\Delta P \to o} f_{on}(\Delta P) = 2W_n \varepsilon_1^2 \tag{2.34}$$

whereas for a forbidden one,

$$\lim_{\Delta P \to o} f_{on}(\Delta P) = o \tag{2.35}$$

This enables spectroscopic identifications to be made.

2.5 Momentum Change for Numerical Calculation

Suppose E_1 and E_2 are the incident and scattered kinetic energies of the electron, given by:

$$E_1 = \tfrac{1}{2} P_1^2 \tag{2.36}$$

and

$$E_2 = \tfrac{1}{2} P_2^2 \tag{2.37}$$

then, the average energy $\bar{E}$ is:

$$\bar{E} = \tfrac{1}{2} (E_1 + E_2) = E_1 - \frac{W}{2}$$

where

$$W = E_1 - E_2 \tag{2.38}$$

then

$$(\Delta P)^2 = P_1^2 + P_2^2 - 2P_1P_2 \text{ Cos } \theta = 2E_1 + 2E_2 - 2(E_1E_2)^{\frac{1}{2}} \text{ Cos } \theta$$

$$= 4\bar{E} - 4(\bar{E}^2 - \tfrac{1}{4} W^2)^{\frac{1}{2}} \text{ Cos } \theta$$

By expanding the bracket in a power series in $\left(\frac{W}{2\bar{E}} \right)^2$ and ignoring terms of order $\left(\frac{W}{2\bar{E}} \right)^4$ and higher,

$$(\Delta P)^2 = 8\bar{E} \left[\left(1-2\left(\frac{W}{4\bar{E}} \right)^2 \right) \text{Sin}^2 \frac{\theta}{2} + \left(\frac{W}{4\bar{E}} \right)^2 \right]$$

when $\frac{W}{\bar{E}} < 0.1$ we have

$$(\Delta P)^2 = 8\bar{E} \left[\text{Sin}^2 \frac{\theta}{2} + \left(\frac{W}{4\bar{E}} \right)^2 \right] \tag{2.39}$$

This approximate formula is in error by a small fraction of a percent when $\frac{W}{\bar{E}} < 0.1$. In the special case $\theta = 0$, $(\Delta P)^2 = \frac{W^2}{2\bar{E}}$ which means at $\theta = 0$ as as $\bar{E}$ becomes large, $(\Delta P)^2$ approaches zero.

2.6 Divergence Errors

In an electron spectrometer, tuned for acceptance of scattered electrons at one particular angle, not all the electrons are deviated through the same angle because of the finite launching and acceptance half angle of the electron spectrometer.

In order to estimate the error, produced by this uncertainty in the scattering angle of the scattered electron beam, Lassettre (1957) has assumed that electrons in the beam have directions uniformly distributed over a cone, with cone angle α. The mean cross-section is obtained from:

$$\bar{\sigma} = \int \sigma d\omega / \int d\omega \tag{2.40}$$

where σ is the cross-section at angle θ and $d\omega$ is an element of solid angle. Suppose:

$$\sigma = \frac{C}{|P_1 - P_2|^2} \tag{2.41}$$

where C is constant. If we choose $\vec{P}_1$ along the Z axis and $\vec{P}_2$ in the XZ plane, after evaluating the integrals, the ratio of $\frac{\bar{\sigma}}{\sigma}$ is

$$\frac{\bar{\sigma}}{\sigma} = \frac{\sin^2 \frac{\theta}{2} + \left(\frac{W}{4\bar{E}}\right)^2}{\sin^2 \frac{\alpha}{2}} \log \frac{S}{T} \tag{2.42}$$

where S and T have the following quantities:

$$S = 2\left[1 + \left(\frac{W}{4\bar{E}}\right)^2\right] \sin^2 \frac{\theta}{2} \tag{2.43}$$

$$T = \left[1+2\left(\frac{W}{4\bar{E}}\right)^2\right] \sin^2 \frac{\theta}{2} - \sin^2 \frac{\alpha}{2} - \left(\frac{W}{4\bar{E}}\right)^2 + \left[\left(\left(\frac{W}{4\bar{E}}\right)^2 + \sin^2 \tfrac{1}{2}(\alpha-\theta)\right) \times \left(\left(\frac{W}{4\bar{E}}\right)^2 + \sin^2 \tfrac{1}{2}(\alpha+\theta)\right)\right]^{\frac{1}{2}} \tag{2.44}$$

In these formulae θ is the angle between the centre line of the incident beam and $\vec{P}_2$. When $\frac{W}{4\bar{E}}$ is negligibly small, and $\sin \frac{\alpha}{2}$ is small compared with $\sin \frac{\theta}{2}$, then (2.42) can be expanded in power of $\frac{\sin \frac{\alpha}{2}}{\sin \frac{\theta}{2}}$

$$\frac{\bar{\sigma}}{\sigma} = 1 + \tfrac{1}{2}\,\frac{\sin^2\frac{\alpha}{2}}{\sin^2\frac{\theta}{2}} + \frac{1}{3}\,\frac{\sin^4\frac{\alpha}{2}}{\sin^4\frac{\theta}{2}} \qquad (2.45)$$

If we ignore the terms of power 4 and higher, then

$$\frac{\bar{\sigma}}{\sigma} = 1 + \tfrac{1}{2}\,\frac{\sin^2\frac{\alpha}{2}}{\sin^2\frac{\theta}{2}} \qquad (2.46$$

or

$$\frac{\bar{\sigma} - \sigma}{\sigma} = \tfrac{1}{2}\,\frac{\sin^2\frac{\alpha}{2}}{\sin^2\frac{\theta}{2}} \qquad (2.47)$$

Table (2.1) gives the values for $\frac{\bar{\sigma} - \sigma}{\sigma}$ derived from equation (2.47) for $\alpha = \frac{1}{4}^{\circ}$.

θ	$\frac{\bar{\sigma} - \sigma}{\sigma}$
1	0.031250
3	0.003473
5	0.001250
10	0.000313
20	0.000078

2.7 Pressure Effect (Double Scattering)

Double scattering has been reviewed by Dillon and Lassettre (1975) and Williams and Willis (1975). The double scattering errors for scattering at low pressure and small scattering angles are negligibly small, but for scattering at high pressure and large angles the effect must be taken into account. Two separate pressure dependent processes are capable of producing errors in the angular distribution of inelastically scattered electrons:

1. An electron, elastically scattered at zero angle, is then inelastically scattered at angle θ.

2. An electron, elastically scattered at non-zero angle, is followed (proceeded) by an inelastically scattering at zero angle (the reverse of 1.). The first effect is negligible. The measured intensity therefore becomes a combination of the intensity I_1, due to single scattering, and I_2, intensity due to double scattering (second case, above).

$$I = I_1 + I_2 \tag{2.48}$$

where
$$I_1 \sim I_o n_o \left(\frac{\partial \sigma \text{ inel.}}{\partial \omega} \right)_\theta \tag{2.49}$$

and
$$I_2 \sim I_o n_o \left(\frac{\partial \sigma \text{ inel.}}{\partial \omega} \right)_o n_o \left(\frac{\partial \sigma \text{ el.}}{\partial \omega} \right)_\theta \tag{2.50}$$

I_o and n_o are the beam intensity and particle density respectively. Hence,

$$I = I_o n_o \left[A\left(\frac{\partial \sigma \text{ inel.}}{\partial \omega} \right)_\theta + B n_o \left(\frac{\partial \sigma \text{ inel.}}{\partial \omega} \right)_o \left(\frac{\partial \sigma \text{ el.}}{\partial \omega} \right)_\theta \right] \tag{2.51}$$

where A and B are proportionality constants depending on electron and atomic beam configuration. The second term of (2.51) indicates the error due to double scattering which is, as seen, proportional to pressure and angle of scattering. The magnitude of this error can be seen from Fig. (2.1). Fig. (2.1) shows the differential collision cross section for elastic (Curve I) and inelastic (Curve II) scattering as a function of the scattering angle. Curve I is much steeper than curve II, therefore, for any particular

Fig. 2.1

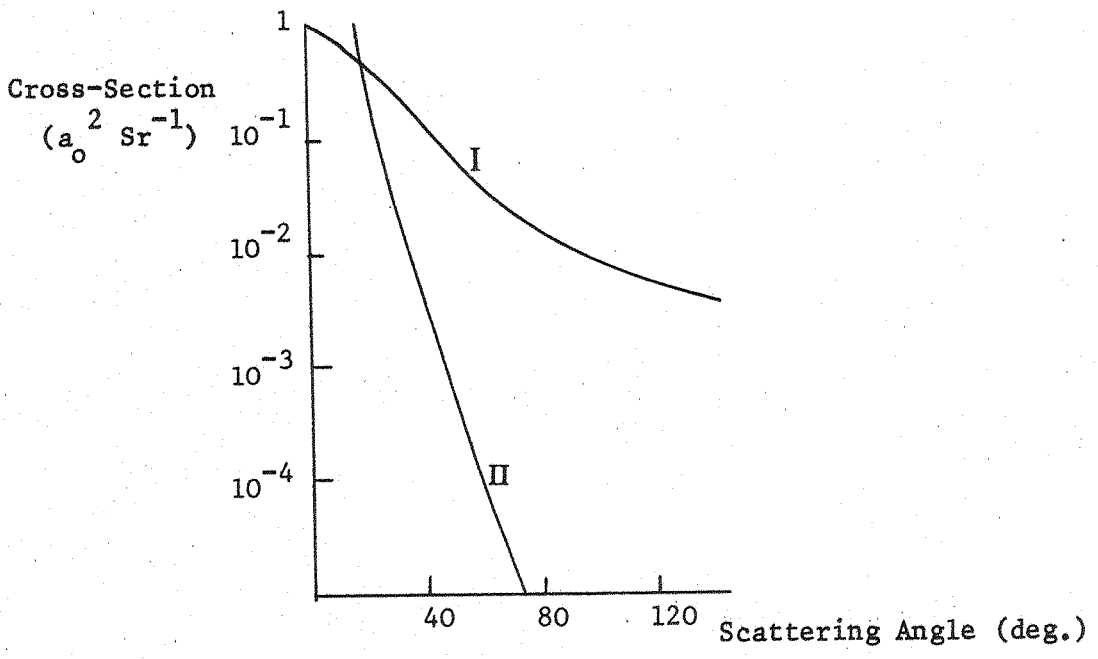

The absolute angular differential cross section for electron losing 10.2 eV in exciting the n = 2 states of atomic hydrogen for 136 eV incident electrons. (Williams and Willis (1975)).

non-zero scattering angle θ, the value of $\left(\frac{\partial\sigma \text{ el.}}{\partial\omega}\right)$ is higher than $\left(\frac{\partial\sigma \text{ inel.}}{\partial\omega}\right)$ and increases substantially with respect to the inelastic cross section with increasing angle. This fact indicates that the second term in (2.51) may become comparable to the first term at high scattering angle (θ) and large pressures (n_o).

Chamberlain and Co-workers (1967) suggested that for single-event electron scattering in static gases the observed scattering intensity, $I(W,\theta)$, is proportional to $I_o P\sigma(W,\theta)(\text{Sin }\theta)^{-1}$ exp. $\left(\frac{-P}{P_o}\right)$ in which I_o is the total current entering the gas cell, P is the pressure, $\sigma(W,\theta)$ is the differential cross-section for unit solid angle for an energy loss W and scattering angle θ, and P_o is a constant inversely proportional to the total cross section. Chamberlain (1967) has defined "low pressure" as that

pressure which might mistakenly be thought adequate to observe only single scattering. Measurements of absolute differential cross-section in helium (Chamberlain, 1967), has shown that a factor of 10 error can be obtained in the 2^1P excitation cross section, at a scattering angle of 20^o and incident energy of 400 eV , when $\frac{P}{P_o} = 1$, due to double scattering.

CHAPTER 3

EXPERIMENTAL

3.1 The Apparatus

Generally, an electron-energy-loss spectrometer requires the following:

1. The production of a beam of electrons of known and controllable parameters, (i.e., energy, energy resolution, angular resolution, etc.).

2. Bombardment of the atomic (or molecular) target by this electron beam.

3. Energy analysis and detection of the resulting scattered electrons.

The energy loss electrons to be detected after scattering, originate from a cathode (in contrast to the ejected electrons in autoionization studies, which originate from the atom). The overall energy resolution of an electron-energy-loss spectrometer is therefore a function of both the incident beam and the electron analyser, used for energy analysis. Typically, the energy from a hot electron emitting cathode (1200^{o}C) is 300 meV. Thus, to achieve an overall resolution of less than 300 meV requires monochromation of the incident beam prior to the interaction region. This is a well established technique and was used for example, by White and Ross (1976) for a high resolution spectroscopic study of discharged hydrogen and nitrogen. However, using this spectrometer for a study of the Generalised Oscillator Strength of the atomic hydrogen 1S → 2P transition, a poor resolution only is required (see chapter 5) and energy monochromation of the incident electron beam is unnecessary. The incident electron beam may therefore be shaped by a simple electrostatic electron gun, capable of producing an electron beam in the energy range 50 to 500 eV and 10^{-6} amperes. The scattered electron beam, requires energy analysis. The same electron optical configuration was used as for the high resolution work of White et al. (1976). The design enables detection of electron-energy loss in the region 0 to 50 eV for incident energies in the range 50 to 500 eV. The design principles are outlined in section (3.8).

3.2 Electron Optic Principles

In any electron beam system, there are two fundamental restrictions which must be satisfied. Consider an electron beam of energy E that passes through a region, defined by two apertures of diameter r and separated by a distance ℓ. The factors which define the current that can be put through these apertures are:

1. Space Charge Forces:

Due to mutual repulsion of the electrons, it is not possible to keep a large number of electrons together in a small volume. The maximum current which can be passed through such a region is:

$$I_{max} = 38.5\ E^{\frac{3}{2}}\ \left(\frac{r}{\ell}\right)^2 \tag{3.1}$$

or, if $\left(\frac{r}{\ell}\right)$ is substituted by the beam half angle α,

$$I_{max} = 38.5\ E^{\frac{3}{2}} \sin^2 \alpha \approx 38.5\ E^{\frac{3}{2}}\ \alpha^2 \tag{3.2}$$

2. Helmholtz-Lagrange Law:

Along any electron beam path where current is conserved, the product of the energy (E), the differential solid angle ($d\Omega$) and the differential area (dA) at any two cross sections 1 and 2 are related by:

$$E_1 d\Omega_1\ dA_1 = E_2 d\Omega_2 dA_2 \tag{3.3}$$

Another form of this formula can be written in terms of the conservation of brightness. "Brightness" or "Richtstrahlwert" is defined as:

$$R = \frac{dI}{dA.d\Omega} \tag{3.4}$$

where dI is the current through a differential area dA and $d\Omega$ is the solid angle. Conservation of current and equation (3.3) gives us:

$$\frac{dI_1}{E_1.dA_1.d\Omega_1} = \frac{dI_2}{E_2.dA_2.d\Omega_2} \tag{3.5}$$

or, with respect to (3.4):

$$\frac{R_1}{E_1} = \frac{R_2}{E_2} \tag{3.6}$$

3.3 Electron Gun

An electron gun is a combination of electrodes for extracting a beam of electrons from an electron source. It consists of: cathode, extraction electrode (anode) to accelerate the electrons away from the cathode, and two or more electrodes, forming an object lens to shape the electron beam.

The field and electron path in the vicinity of the cathode of an electron gun are very complex. This makes the exact design of electron guns necessarily, at least, partly empirical. The principle matter in electron gun design is producing an electron beam cross-over of small diameter, small angular resolution and high current density. A serious limiting factor in the production of a small electron beam image is the space-charge mutual electrostatic repulsion between electrons in the beam, which prevents electrons of the beam coming together into a point focus. This effect perdominates for low electron energies and seriously limits the maximum current available from a low energy electron gun.

Let us consider the diode gun to illustrate the limitation of electron gun design.

3.3.1 Properties of the Diode Gun

The diode is the simplest electron gun. It is an extraction stage only, and is shown in Fig. (3.1). The electron field between the anode and the cathode under space-charge condition is:

$$\varepsilon(\psi) = \frac{4V_A}{3d^{4/3}} \psi^{1/3} \qquad (3.7)$$

where ψ is distance from cathode, d is separation of cathode (K) and anode (A) and VA is the anode potential (Kuyatt, 1967). The entrance and exit window of the gun is the anode hole itself. Since the entrance window is formed by parallel rays, the input pupil is at $-\infty$ and the exit one is at $-f = -3d$. The sizes of input pupil and anode hole are: $r_c = 3d\theta_p$ and $r_A = 3d\theta_B$ respectively, where θ_B is the beam angle, and θ_p is the maximum angle of rays reaching the anode hole. θ_p is given by:

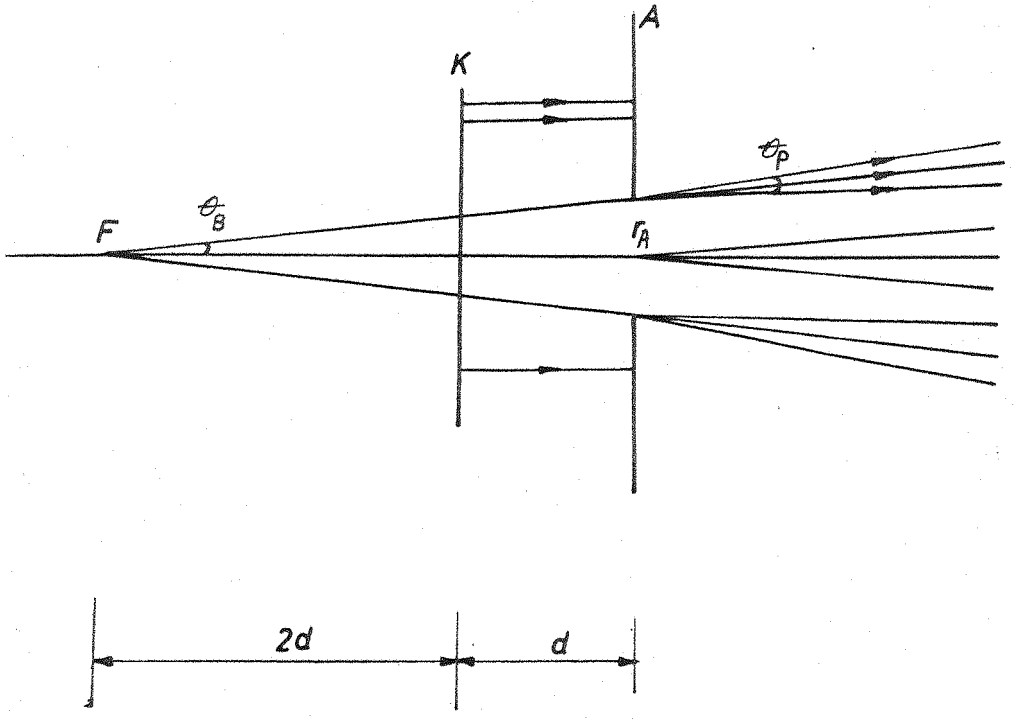

Fig. 3.1 Diode Characteristics

$$\theta_P = \sqrt{\frac{V_K}{V_A}} \tag{3.8}$$

where $$V_K = K\, T_M \tag{3.9}$$

K is constant and T_M is the cathode temperature.

The space-charge limited current from such a diode is (Kuyatt, 1967):

$$J_{max} = K\, \frac{V_A^{\frac{3}{2}}}{d^2} \tag{3.10}$$

where K is a constant.

Another limitation factor in the maximum attainable current density from a thermionic cathode is a thermal effect and may be derived from consideration of the Helmholtz-Lagrange law. From equation (3.5) we obtain:

$$J_{2_{max}} = J_1\, \frac{E_2}{KT} \tag{3.11}$$

This relation must hold between the plane of the cathode and the plane of smallest beam diameter. Here, KT cannot be made infinitely small (300 m.e.v. typically for a cathode operated at 1200°C) and J_1 is limited by space-charge. In this way, space-charge and thermal effect limit gun design generally. Therefore the technique of multi-staging or multi-anoding the electron gun, particularly for low energy guns, is used.

3.3.2 Multistage and Multianode Guns

In the multistage guns which were first used by Simpson and Kuyatt (1966), a high extraction voltage was used for the anode, and the beam then decelerated to the required operation energy. This technique has the advantage of isolating the extraction voltage from the final operation voltage of the gun. Consequently, the extraction energy may be made sufficiently large (independently of operation energy) to attain a large electron beam current (given by equation 3.1). Many electron guns, using this technique, have been used very successfully (see for example, Simpson and Kuyatt, 1963). The most versatile guns usually have a three element lens deceleration stage.

This enables the operational energy to be varied independently of the extraction energy. The two element deceleration stage has a fixed operational energy ratio for fixed object and image position (see section 3.4.1) and therefore necessitates simultaneous adjustment of extract energy with operation energy. A further sophistication to electron gun design is the use of a triode extraction stage. In this extraction stage, the extra electrode (bias or gird) placed between anode and cathode can be used to produce a convergent electron beam (divergent beam from diode) focussing to a position in front of the anode. Location of this focus position may be varied with grid potential. The grid, therefore, becomes a useful tuning device for the whole gun assembly.

Further, the diode depends critically on cathode-anode spacing (d). With the additional bias any small construction errors may be compensated with the bias potential. The design of such extraction stages is based on the empirical data of Soa (1959).

3.3.3 The Gun in this Experiment

The gun, used in this experiment, utilised a modified 3K/5U high energy gun made by Superior Electronics. It consisted of an indirectly heated cathode, bias, anode, three element lens and deflector set. The complete gun assembly was supported on axis by four ceramic rods.

The indirectly heated cathode was oxide coated tungsten, mounted on a ceramic button and held rigidly inside the bias housing. In practice, the deflectors were not used for two reasons:

1. There was a shortage of space for mounting the gun.

2. The deflectors, at the end of the gun, did not match the carefully designed entrance aperture of the scattering chamber which was designed for minimum gas leakage (see section 3.9). Therefore, the gun was shortened by removing the deflectors, and a two element lens and shorter deflector set were used in their places. The complete gun, with extra lens and deflectors

is shown in Fig. (3.2). It was found to produce an electron beam current in excess of 1 μA. for all energies above 50 eV.

Operating voltages and currents for the modified gun are outlined in Table (3.1).

TABLE (3.1)

Typical Operating Voltages and Currents for the Modified Gun (for 500 meV Resolution)

ENERGIES (eV)						CURRENTS (μA)				
Beam Energy	Bias	A_1	A_2	A_3	L_1	A_1	L_2	W_o	W_1	W_2
400	-4	400	50	250	70	20	-	11	0.2	1.2
200	-4	400	56	113	56	20	-	12	0.3	1.0

Note:

Larger values of current are obtainable by altering the bias voltage. For a detailed discussion of the effect of bias voltage on resolution, see section (4.4).

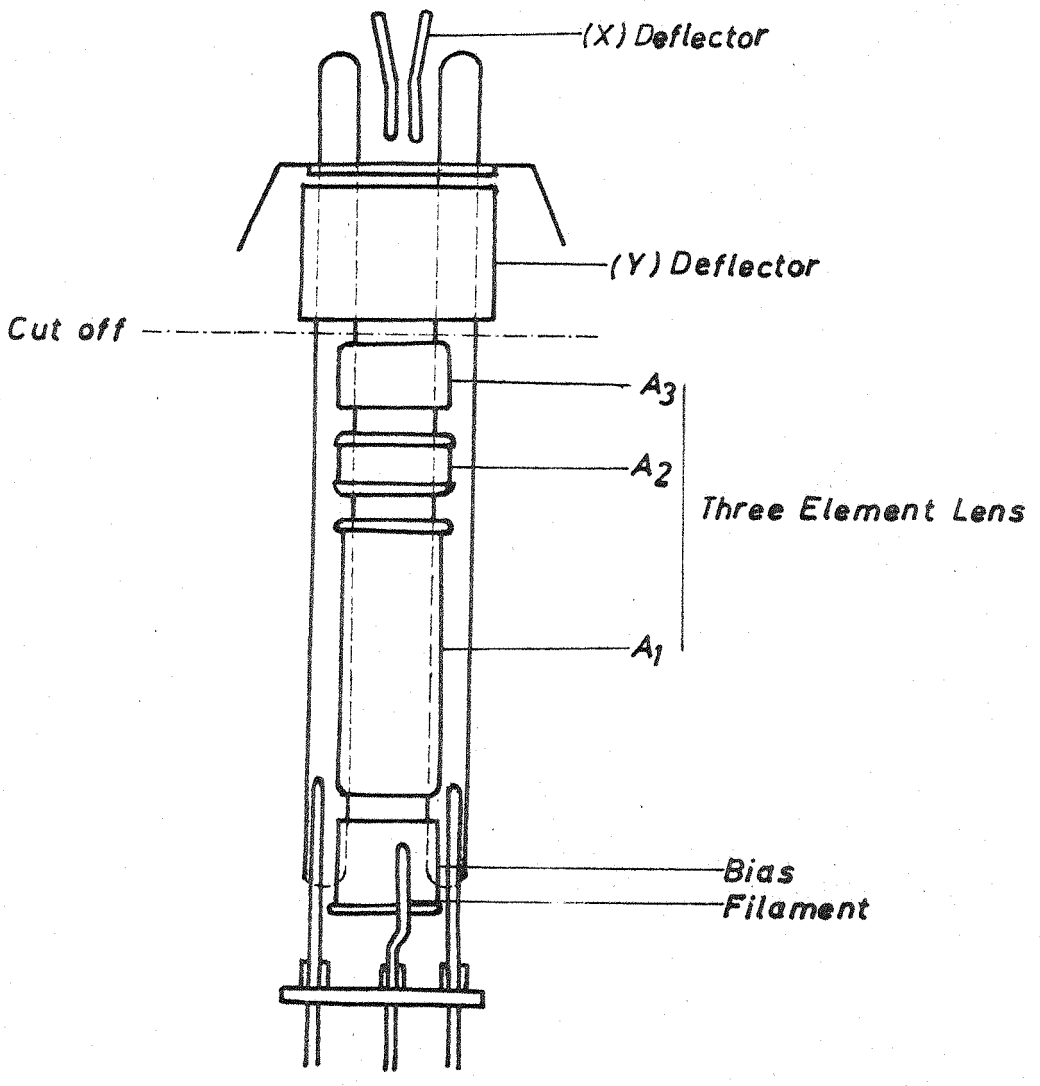

Fig. 3.2 3K/5U Electron gun

3.4 ELECTRON LENSES

The shaping and transport of an electron beam to obtain the correct spot size, angular collimation and energy, is achieved with the aid of electrostatic electron lenses. The resulting electrostatic potential distribution produced by two electrodes, maintained at different potentials V_1 and V_2, creates a refracting surface to incident electrons analogous to an optical lens (See Fig. 3.3). Its properties may therefore be discussed in terms of the thick lens notations of optical physics (see Fig. 3.4).

3.4.1 Properties of Two Element Electron Lenses:

The properties of the lenses may be reduced to a number of cardinal points which are as follows:

P_1 and P_2 (principal points) are the interaction of incident and refracted rays, (or their extensions). Two planes, passing through these two points, and perpendicular to the axis, are principal planes. In real life, these two planes coincide and are located on the low voltage side of the lens.

F_1 and F_2 are focal points whose positions are measured with reference to the mid plane M.

f_1 and f_2 (focal lengths) are focal distances from the relevant principal planes.

P and q are the distances of object and image from mid plane M.

y_1 and y_2 are the sizes of object and image respectively.

θ_1 and θ_2 are the half angles that rays make with the axis.

3.4.2 Thick Lens Equations

The relationship between lateral magnification ($M = \frac{y_2}{y_1}$) and angular magnification ($m = \frac{\theta_2}{\theta_1}$) is given by the Abbe-Helmoltz law:

$$\sqrt{V_1}\, y_1 \sin\theta_1 = \sqrt{V_2}\, y_2 \sin\theta_2 \qquad (3.12)$$

which may be written as:

$$m.M = \sqrt{\frac{V_1}{V_2}} \qquad (3.13)$$

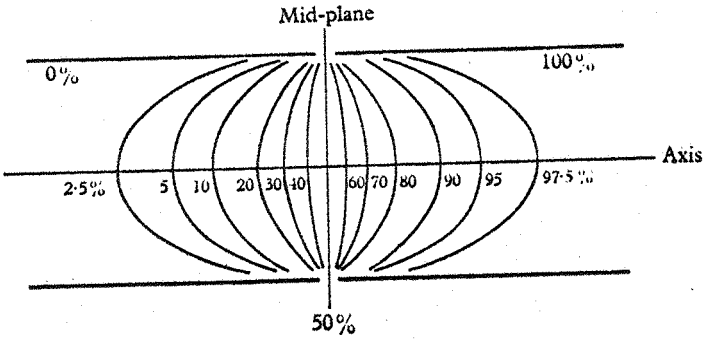

Fig. 3.3

Potential distribution in symmetrical two tube lense
(Klemperer and Barnett, 1971)

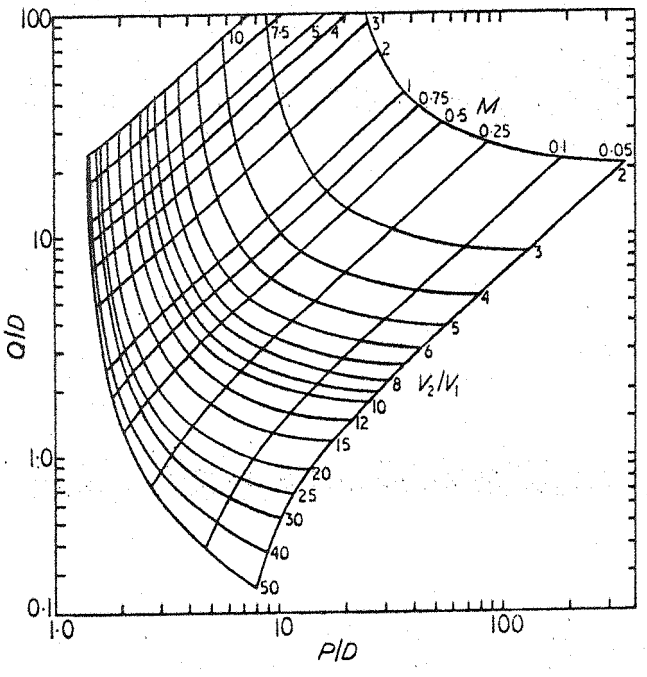

Fig. 3.5

Values of the conjugate object image points and magnification for g/D=1.0
(Read, Adams, and Soto-Montiel, 1971)

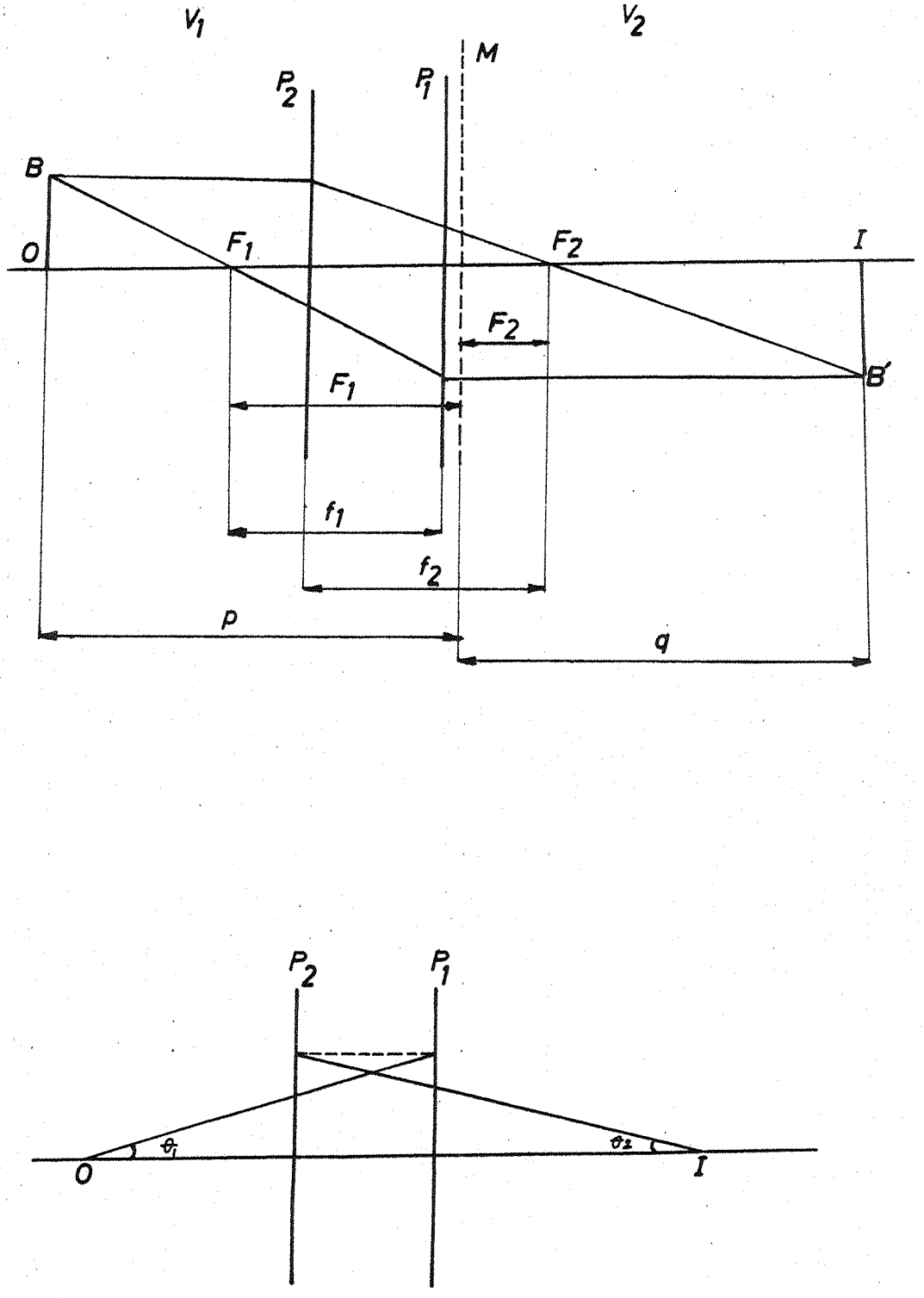

Fig. 3.4 Cardinal points of a two element electron lens.

the relationship between two focal lengths can be derived from Newtonian lens equation (see for example, Klemperer and Barnett, 1971):

$$\frac{y_2}{y_1} = -\frac{f_1}{p} = \frac{-q}{f_2} \tag{3.14}$$

$$f_1 f_2 = pq \tag{3.15}$$

If $U = p + f_1$ and $v = q + f_2$, object and image distances from the appropriate principal points, then we will have:

$$(U - f_1)(v - f_2) = f_1 f_2 \; ; \; \frac{f_1}{u} + \frac{f_2}{v} = 1 \tag{3.16}$$

Thus a knowledge of f_1 and f_2 is required for the design of a two element lens.

Two element lenses are known as positive lenses because they always make the electron beam more convergent, whether they accelerate the beam ($V_2 > V_1$) or decelerate it ($V_1 > V_2$).

Calculated properties of two element lenses are often presented in the form of graphically conjugate object and image focussing positions (P - q curves). These curves represent equations P and q graphically and provide easy reference for the design of lens systems. An example of these sort of curves is shown in fig. (3.5) in which $\frac{q}{d}$ is plotted against $\frac{P}{D}$ for different values of $\frac{V_1}{V_2}$ and for constant magnification values. D is the lens diameter (Read, Adams and Soto-Montiel 1971, Heddle 1969, Spangenberg and Field, 1943).

3.4.3 Three Element Lenses

For a fixed object and image position with a discrete energy ratio, focussing is obtained with only a two element lens. However, on many occasions electron-energy-loss spectroscopy requires fixed imaging distances for variable energy ratios. This may be achieved with a three element lens. The central electrode now splitting the lens system into effectively two two element lenses with energy ratios of $\frac{V_1}{V_2}$ and $\frac{V_2}{V_3}$. The central

electrode potential (V_2) therefore provides the variable focus for various outer electrode energy ratios $\frac{V_3}{V_1}$ to maintain fixed object and image distances.

The simplest method of deducing three element lens characteristics is to divide it into two successive two-element lenses. By using two element lens characteristics which are well known, the three element lens characteristics may be calculated (see for example, Heddle, 1969, and Kuyatt, 1967).

This method utilizes the property that eight points on the three element lens focal locus may be predicted from well known two element lens data. This is shown by Heddle (1969). A typical focal locus is shown in Fig. (3.6). Points B,D,F and H correspond to two adjacent electrodes, having the same potential, reducing lens to a two element one. The remaining four points A,C,E and G relate to a parallel ray path in the centre element of the lens. The object and image therefore correspond to the focal points of the two two-element lenses concerned. As might be expected, each energy ratio $\frac{V_2}{V_1}$ has two focussing points for $\frac{V_3}{V_1}$. These are the upper and lower focus modes of the lens. This technique provides reasonable accuracy in predicting the focal locus for any three element cylindrical lens.

The dependence of the magnification on the overall energy ratio of three element lens may also be calculated and plotted (fig. 3.7), using the technique suggested by Heddle and Kurepa (1970).

The eight points, indicated on this curve (in fig. (3.7), refer to the corresponding points of the focal locus curve, shown in fig. (3.6). A complete set of electron optical lens data has been published recently by Harting and Read (1976).

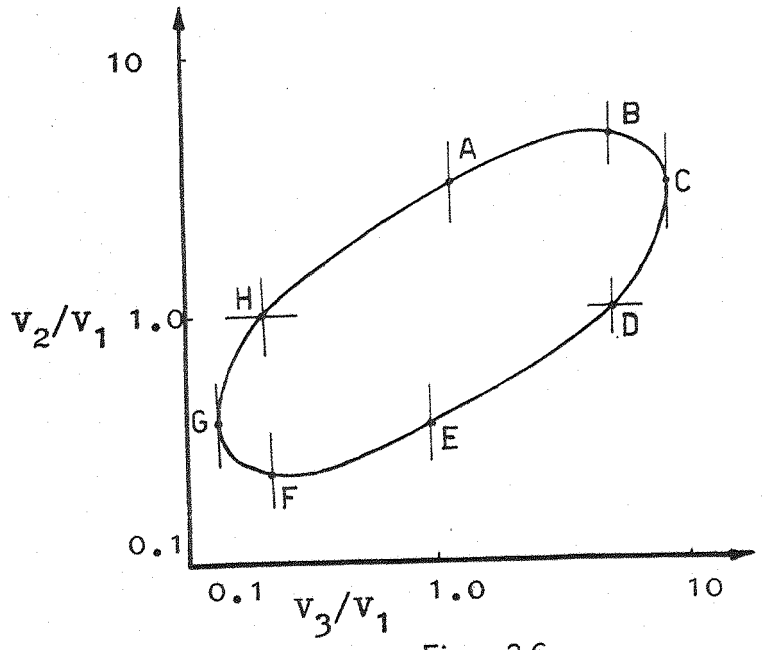

Fig. 3.6

Focal locus for three element lens with L_1=5.0D, L_2=3.0D, L_3=6.0D and separation gap 0.1D
(Heddle, 1969)

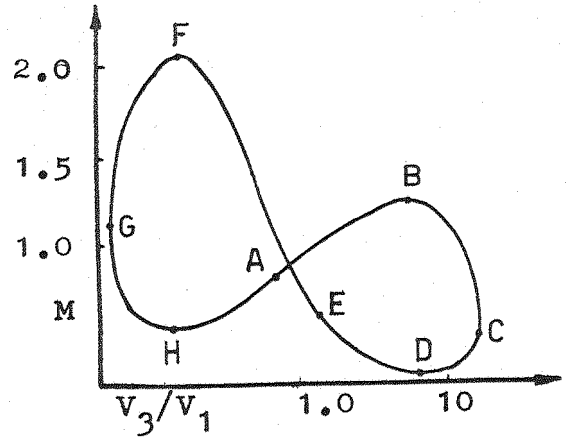

Fig. 3.7

Calculated magnification of a lens with L_1=4.37D, L_2=3.85D, L_3=3.06D and separation gap 0.1D
(Heddle and Kurepa, 1970)

3.5 Electron Energy Analyser

Electron energy analysers take many forms: electrostatic, magnetic, or a combination of the two, many of which have been used in different experiments (see for example, Dillon et al. 1975 and Kuyatt et al.1967). In the present experiment, the hemispherical analyser was used. It has the advantage of three dimensional focussing.

Aston (1919) was one of the first people to suggest using a portion of a spherical condenser as an electron energy analyser. The principle of the hemispherical velocity analyser relies on Kepler's first law of planetary motion: "Particles with the same total energy, in a given field, have the same major axis".

In the hemispherical analyser an inverse square radial electrostatic field is produced by a potential difference applied between two concentric hemispheres. The resulting properties are discussed below.

3.5.1 The Properties of the Hemispherical Electron Velocity Analyser

The hemispherical electron velocity analyser is schemetically shown in fig. (3.8). The radii of two hemispheres are R_1 and R_2 ($R_2 > R_1$). The potentials on the outer and inner hemispheres which produces a $\frac{1}{r^2}$ electrostatic field for transmission of electrons are:

$$V_1 = 2V_o \left(\frac{R_2}{R_1} - \frac{R_o}{R_2}\right) \; ; \quad V_2 = V_o \left(\frac{R_2}{R_1} - 1\right) \tag{3.17}$$

these equations are discussed later (see section 3.5.2).

Hence the potential difference between the two hemispheres is:

$$V = V_o \left(\frac{R_2}{R_1} - \frac{R_1}{R_2} \right) \tag{3.18}$$

The energy resolution for this system is (Kuyatt and Simpson, 1967, see section (3.5.3.)):

$$\Delta E_{\frac{1}{2}} = E_o \left(\frac{W}{2R_o} + \alpha^2 \right) \tag{3.19}$$

Here, W is the width of entrance and exit apertures of the system, E_o is

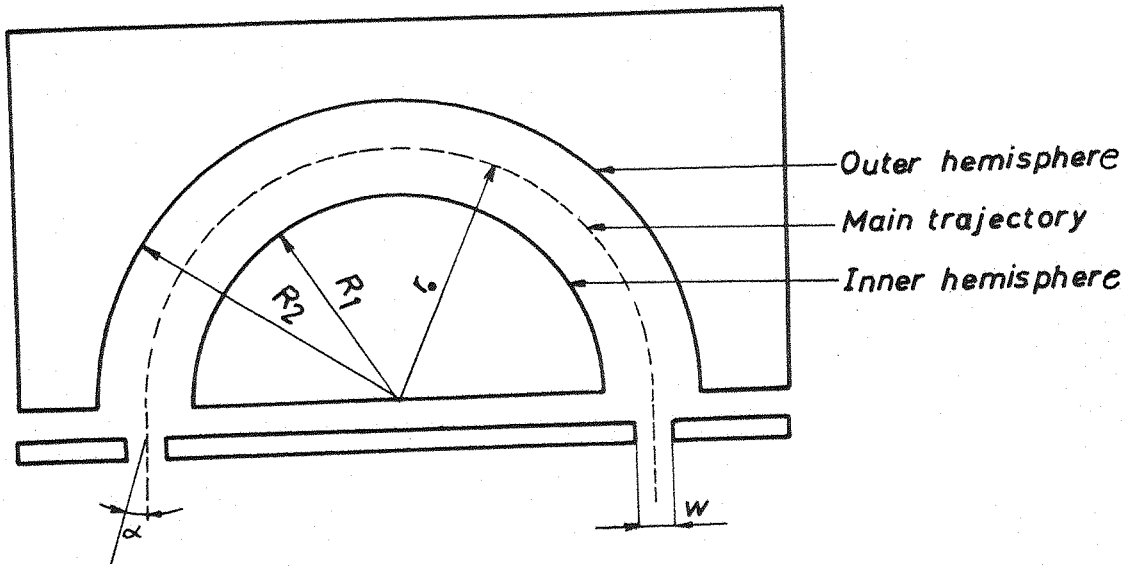

Fig. 3.8 Schematic diagram of the hemispherical electron velocity analyzer

the energy of the electron which traverse in the path R_o; R_o is the mean radius:

$$R_o = \frac{R_1 + R_2}{2} ;$$

α is the angular divergence of the beam.

The maximum current that may be transmitted by the analyser is limited by space-charge and is given by (see section 3.2):

$$I = 38.5\, E_o^{\frac{3}{2}}\, \alpha_o^{\,2} \tag{3.20}$$

3.5.2 Calculation of Hemisphere Operating Potentials

The electrostatic field at a radius r which is produced by a potential difference between two hemispheres is governed by:

$$E = \frac{K}{r^2} \tag{3.21}$$

where K is a constant. If V is the electric potential, we have

$$E = -\frac{dV}{dr}$$

or

$$V = \frac{K}{r} + C \tag{3.22}$$

Applying the boundary conditions:

$$V_1 = \frac{K}{R_1} + C \quad \text{and} \quad V_2 = \frac{K}{R_2} + C \tag{3.23}$$

so;

$$V_1 - V_2 = K\left(\frac{1}{R_1} - \frac{1}{R_2}\right) \tag{3.24}$$

$$K = \frac{V_1 - V_2}{\frac{1}{R_1} - \frac{1}{R_2}} \tag{3.25}$$

and

$$C = -\frac{V_1 - V_2}{R_1\left(\frac{1}{R_1} - \frac{1}{R_2}\right)} + V_1 \tag{3.26}$$

the force, F, on a charged particle in an electrostatic field is:

$$F = eE \tag{3.27}$$

and the centrifugal force on a particle when it travels in a circular path is:

$$F = - \frac{m v^2}{r} \tag{3.28}$$

(v is the velocity and r is the path diamater). When the electrostatic force is equal to the centrifugal force:

$$eE = - \frac{m v^2}{r} = -e \frac{K}{r^2}$$

and therefore:

$$v^2 = \frac{e}{m} \frac{K}{r} \tag{3.29}$$

the kinetic energy of electron is:

$$E_K = \tfrac{1}{2} m v^2 = e V_o \tag{3.30}$$

From equations (3.29) and (3.30):

$$E_K = \frac{eK}{2r} \tag{3.31}$$

and from equations (3.25) and (3.31):

$$E_K = eV \frac{R_1 R_2}{R_2^2 - R_1^2} \tag{3.32}$$

and

$$e V_o = e V \frac{R_1 R_2}{R_2^2 - R_1^2}$$

or

$$V = V_o \left(\frac{R_2}{R_1} - \frac{R_1}{R_2} \right) \tag{3.33}$$

Hence, the potentials of the inner and outer hemispheres, V_1 and V_2 respectively, are:

$$V_1 = 2V_o \left(\frac{R_2}{R_1} - \frac{R_o}{R_2} \right) \tag{3.34}$$

and

$$V_2 = V_o \left(\frac{R_2}{R_1} - 1 \right) \tag{3.35}$$

3.5.3 Resolution of a Hemispherical Velocity Analyser

The resolution of a spherical sector analyser has been discussed by Purcell (1938). Fig. (3.9) shows a cross-section of a spherical analyser in which electrons of energy E_o entering at point P are transmitted along radius r_o to point Q provided the inner and outer hemispheres have potentials given by (3.17).

If electrons with an energy different from E_o, say $E_o + \Delta E$, enter at P, they are not focussed to the point Q, but to a point S, where:

$$QS = Y \tag{3.36}$$

Y is given by:

$$Y = \beta \, r_o \left(1 + \frac{q}{p}\right) \tag{3.37}$$

where

$$\beta = \frac{\Delta E}{E_o} \tag{3.38}$$

therefore:

$$\frac{\Delta E}{E_o} \quad \frac{Y}{r_o\left(1 + \frac{q}{p}\right)} \tag{3.39}$$

the energy ef electrons, transmitted by this analyser is defined by placing a slit in the exit plane. If the width of such a slit is W, then the resolution of the analyser will be:

$$\frac{\Delta E}{E_o} = \frac{W}{r_o\left(1 + \frac{q}{p}\right)} \tag{3.40}$$

An electron with energy E_o which travels along PK, which is making an angle α with PT, will not reach the point Q, but a point S', a distance Y' from Q;

$$QS' = Y' \tag{3.41}$$

Y' is proportional to α,

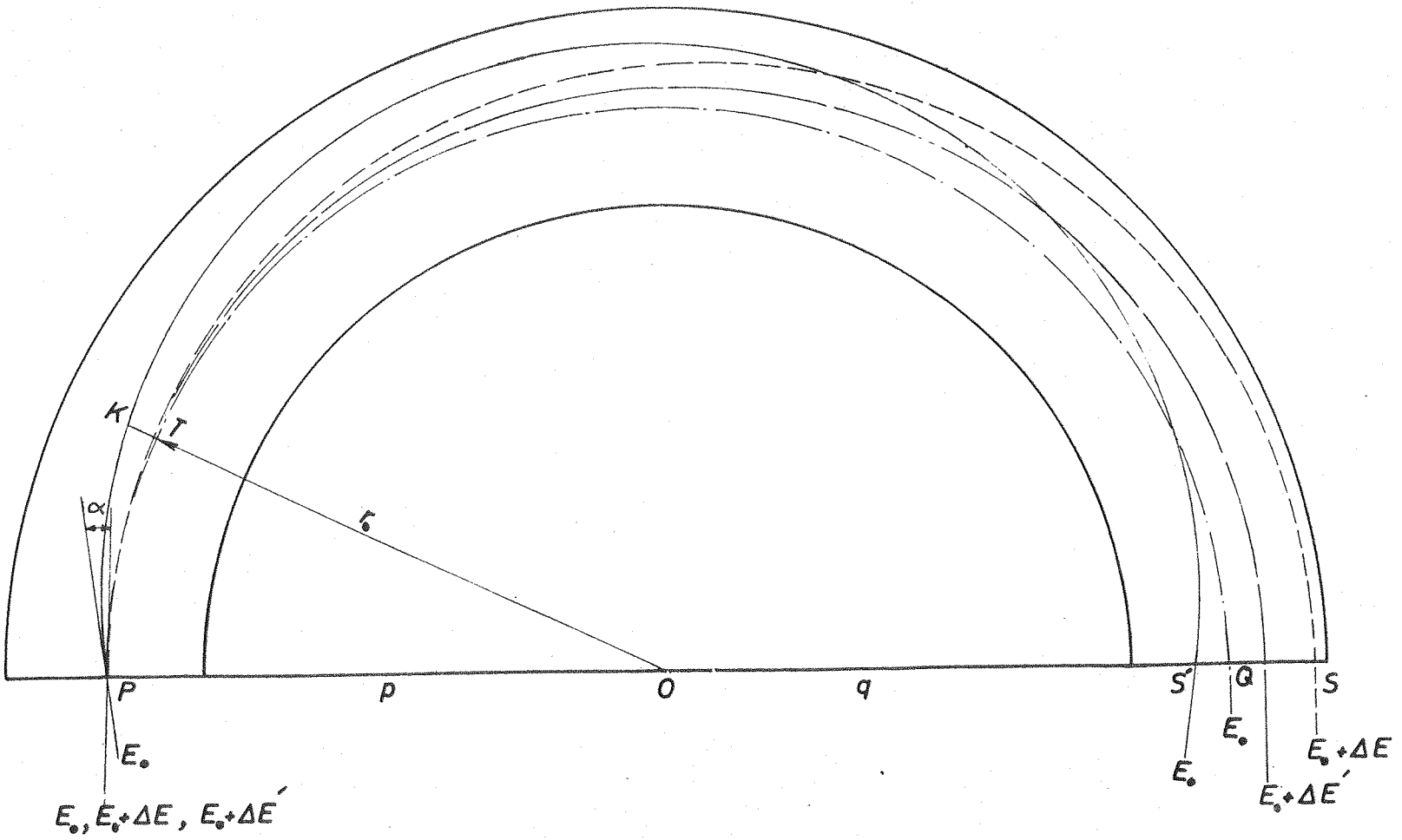

Fig. 3.9 Transmission of electron beam in hemispherical analyzer

$$Y' = -\alpha^2 r_o \left(\frac{p^2}{q^2} + \frac{q}{p} \right) \tag{3.42}$$

Knowing Y', $\Delta E'$ can be calculated:

$$Y' = \beta' r_o \left(1 + \frac{q}{p} \right) \tag{3.43}$$

where

$$\beta' = \frac{\Delta E'}{E} \tag{3.44}$$

therefore

$$\frac{\Delta E'}{E} = \frac{Y'}{r_o(1 + \frac{q}{p})}$$

or

$$\frac{\Delta E'}{E} = \frac{-\alpha^2 r_o \left(\frac{p^2}{q^2} + \frac{q}{p} \right)}{r_o \left(1 + \frac{q}{p} \right)} \tag{3.45}$$

the slit serves to separate rays of different energies, and, due to the imperfect focussing, electrons at different angles α to the normal ray. Therefore:

$$\frac{\Delta E}{E_o} + \frac{\Delta E'}{E_o} = \frac{W}{r_o(1 + \frac{q}{p})} \tag{3.46}$$

and thus:

$$\frac{\Delta E}{E_o} = \frac{W}{r_o(1 + \frac{q}{p})} + \frac{r_o \alpha^2 \left(\frac{p^2}{q^2} + \frac{q}{p} \right)}{r_o \left(1 + \frac{q}{p} \right)} \tag{3.47}$$

which leads to:

$$\frac{\Delta E}{E_o} = \frac{W}{r_o \left(1 + \frac{q}{p} \right)} + \alpha^2 \left(1 - \frac{p}{q} + \frac{p^2}{q^2} \right) \tag{3.48}$$

The second term has got its minimum value for $q = 2p$.

In case of the hemispherical analyser, p = q, and the resolution is therefore given by:

$$\frac{\Delta E}{E_o} = \frac{W}{2r_o} + \alpha^2 \tag{3.49}$$

3.5.4 Analyser in the Present Experiment

The energy analyser, used in this experiment, was an electrostatic 180^{o} hemispherical with dimensions as following:

$$R_1 = 51.3 \text{ mm.} \qquad R_2 = 64.1 \text{ mm.} \quad \text{and} \quad R_o = 56 \text{ mm.}$$

the hemispheres were made of copper with real entrance and exit apertures. In order to reduce secondary electrons, produced in the analyser, and to ensure equipotential surfaces, the surfaces of the hemispheres were coated with a homogeneous thin layer of colloidal graphite solution (Dag.).

Using the analyser resolution equation (3.19) and the analyser dimensions listed below, the resolution may be calculated:

$$W = 0.5 \text{ mm.}, \quad R_o = 56 \text{ mm.}, \quad \alpha_o = 0.047 \text{ radians}$$

$$\frac{\Delta E}{E_o} = \frac{W}{2R_o} + \alpha_o^{\,2} = 0.0067$$

therefore, if $E_o = 10$ eV, then $\Delta E = 67$ meV and for $\Delta E = 30$ meV, $E_o = 4.5$ eV.

3.6 Scattered Electron Analysing Operation

The resolution of the analyser is given by equation (3.19) and therefore, high resolution demands a low analysis energy E_o. The scattered energy-loss electrons are generally high energy (i.e. 200 eV incident energy electrons with typically 10 eV energy loss) and the energy-loss spectrum can be obtained by tuning the analyser to the energy of these scattered electrons. This has the disadvantage of both poor and variable resolution throughout the energy loss spectrum. To accommodate these two features, a two stage system was used to decelerate and focus the scattered electons into the hemispherical analyser at a constant low energy. This system combined a two and a three element electron lens. The two element electron lens (L 6/7);

$$(P = 2.3D,\ q = 2.3D\ \frac{V_2}{V_1} = 14,\ D = 17.22 \text{ mm.})$$

was used simply to decelerate the beam by a fixed amount, whilst the three element lens ($L_{3/4/5}$):

$$(L_3 = 4.0D,\ L_4 = 2.5D,\ L_5 = 3.0D\ \ D = 7.69 \text{ mm.})$$

was used to provide variable focussing over a range of scattered electron energies. (The principles of two and three element lenses are discussed in section (3.4)). A schematic diagram of the configuration, used, is shown in Fig. (3.10).

Typically, the analyser is tuned only for the transmission of, say 10 eV electrons; only 140 eV electrons reaching the object (w_3) of the two element lens $L_{6/7}$ will therefore be transmitted through the analyser. The three element lens is capable of accelerating or decelerating to 140 eV and focussing through w_3 electrons of energy 50 to 500 e.v. (incident energies of 100 - 500 eV with energy losses of 0 - 50 eV).W_2, W_3 and W_4 were the real windows of the system. W_4 of size 0.33 mm. defined the entrance window of the analyser, W_1 and W_2 were used only to reduce gas leakage

Fig. 3.10

SCHEMATIC DIAGRAM OF THE SPECTROMETER

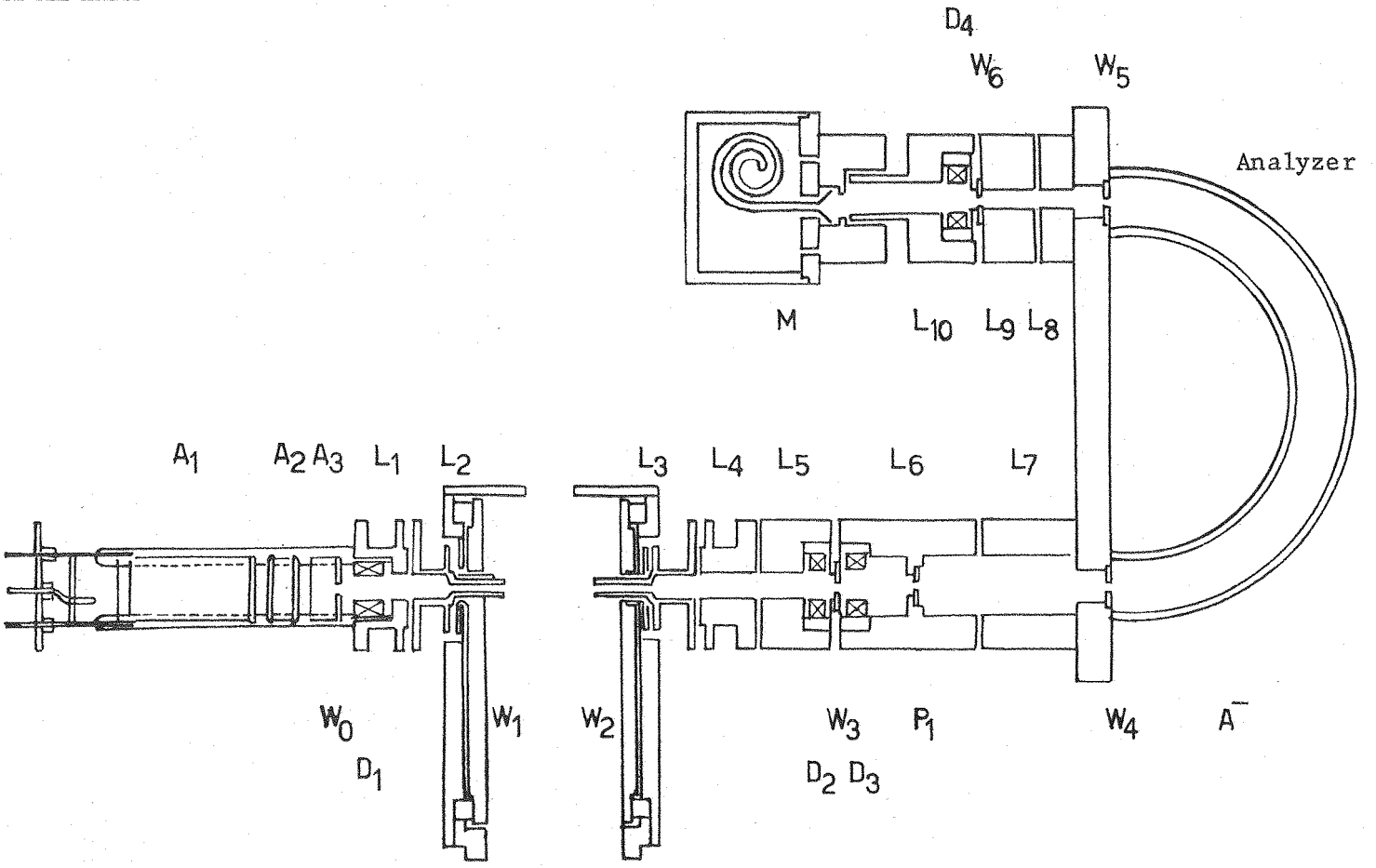

(see section 3.9). W_3 was merely a beam stop to prevent any electrons having hit lens walls being transmitted. The pupil, p_1, sets the correct half angle for operation of the analyser, according to equation (3.49). Following energy analysis, the transmitted electrons are re-accelerated into a drift tube prior to detection by a channel electron multiplier. A two element lens ($L_{8/9}$) was used for this purpose.

$$(p(L_8) = 4.5D \quad q(L_9) = 3.0D \quad \frac{g}{D} = 0.1 \quad \frac{V_2}{V_1} = 8)$$

The electron energy loss spectrum is obtained by scanning the potentials on the element L_4 and L_5, using an electronic ramp generator, to bring the electron energy at w_3 to 140 eV The resulting multiplier signal is recorded as a function of the ramp voltage, applied to L_5 and displayed on a X-Y recorder.

Simultaneous variation of the potential applied to L_4, the focussing electrode of the three element lens, maintained the focus of the three element lens for transmission of the beam through w_3 for a wide range of scattered electron energies.

Typically electron beam energies at various stages in the electron optics are tabulated following:

Beam Energy

L_3	L_4	$L_{5/6}$	$L_{7/8}$	$L_{9/10}$
400/200 eV	Slight Variation of 20 eV	150 eV	10 eV	60 eV

the current at L_3 was typically of the order 10^{-6} amps.

3.7 Vacuum System

Two pumping stacks were used for this experiment. The main pumping stack was used to obtain a good pressure in the main chamber for operation of the electron gun and reducing background scattering to a minimum. This consisted of a liquid nitrogen trapped six inch mercury diffusion pump and water cooled chevron baffle. A Metrovac rotary vacuum pump was used. The background pressure in the vacuum chamber was typically 5×10^{-8} torr.

A similar pumping stack was used for gas handling. In this case the chevron baffle was removed and a faster rotary backing pump ($250 \frac{\ell}{\text{min}}$) was used to provide the pumping speeds necessary to transport the transient species of discharged afterglows from the discharge cavity to the interaction region (scattering chamber) quickly.

Both pumping stacks could be isolated from the main vacuum chamber by means of butterfly valves. The pressure of the main pump stack and the vacuum chamber were measured with "V.G ." ionization gauge heads. Backing pressures were measured with "Edwards" pirani gauges. The chamber could be baked with heating strips on the outside of the chamber, and internally with heating bulbs. This enabled a better vacuum to be maintained, and resulted in a more stable electron optical system.

3.8 Construction

The vacuum chamber which enclosed the electron optical system and scattering volume, was cylindrical, made of non-magnetic stainless steel type EN 58J. It was of 56 cm. diameter and 34 cm. depth. The lens electrons were mounted on two dural HP30 optical benches. One of these, the electron gun, was attached to the base plate of the vacuum tank. The analyser section was mounted on a rotating plate. The rotating plate was mounted on nine ball bearing races. Rotation of the plate from outside the chamber was achieved by a rotary lead through type R 850 made by V.G..

Most of the electron optical elements, except L_2 and L_3, were made of copper to a tolerance of ± 0.05 mm. These lens elements were insulated from the optical bench by 6 mm. diameter ceramic rods. The deflectors and the analyser were insulated from the bench by ceramic washers. L_2 and L_3 were made of titanium to provide the added strength required for driving the scattering chamber (see section 3.9). They were attached to the scattering chamber by flexible bellows to complete the leak free scattering chamber.

The hemispherical analyser was mounted on an optical bench which itself was fixed to the rotatable platform. Ceramic washers were used for insulation. Excessive care had to be taken in order that all the lens elements were correctly aligned.

The hemispherical analyser was dowelled into position on the optical bench.

Alignment of the incident and scattered electron optics were obtained with a specially made alignment tool which ensured a correct mechanical zero angle position. A height gauge was used to ensure that the axis of the electron optical system remained at the same height above base plate through the entire electron optical path.

3.9 Scattering Chamber

The scattering chamber consisted of two cylinders; an outer cylinder which was fixed to the tank base, and an inner cylinder which was movable. The 0.5 mm. gap between the two cylinders was bridged with P.T.F.E. sleeve to both ensure smooth movement in vacuum and prevent gas leakage. The inner cylinder was supported by a thrust bearing. The slotted holes on the inner and outer cylinders allowed passage of lenses L_2 and L_3 and rotation of L_3 between -7° to $+20^{\circ}$ with respect to the incident electron beam direction. The scattering chamber entrance and exit windows (W_1 and W_2) diameters were 0.5 mm. to reduce the gas leakage from the scattering chamber. Two bellows linked the lens elements L_2 and L_3 and the scattering chamber. Apart from minimizing gas leakage from the scattering chamber, the bellows also allowed adjustment of the lens elements on the optical benches.

3.10 Target Element

The gas was taken directly from a cylinder. The flow rate was controlled by a leak valve. A combination of 12 and 16 mm. Pyrex glass tubing was used to guide the gas from the leak valve to the scattering chamber. Along the vertical part of this tube, at a distance of 400 mm. from the scattering chamber, the discharge cavity was fixed. The inlet gas pressure was monitored on a pirani gauge. Production of the discharge was achieved by a 2450 MHz electrodeless microwave discharge cavity, clipped on to the glass tube. The power was supplied by a Microton 200 power unit. The discharge was initiated with a tesla coil and the cavity was cooled by air, blowing from a compressor.

3.11 Operation of the Spectrometer

A filament voltage of 11 volts was sufficient to supply a current of 1 μA to the scattering chamber. The incident beam was tuned by adjusting A_1,A_2 and A_3 such that the beam current was maximised on to W_2. Gas was then introduced into the scattering chamber. Under normal operating conditions, this caused a rise in the background pressure to 8×10^{-7} torr. The pressure of the gas at the inlet was monitored to be approximately 80 m. torr. This corresponds to a calculated scattering chamber pressure of approximately 1 to 2 m.torr. The scattering chamber pressure could not be monitored. This pressure was the lowest that could be used in order to maintain the discharge.

Due to the large intensity of the beam at zero scattering angle, it was necessary to work at scattering angles of 5^{o} and higher in order that only scattered electrons were transmitted through the window W_2. At zero scattering angle, the unscattered beam was too high for the multiplier, causing saturation. The analyser was set up to transmit electrons of 10 eV energy.

In order to tune the scattered beam electron optics, the largest or resonance transition of the element being studied was chosen, for example in helium the 21.21 eV transition. Thus for a 500 eV incident electron beam, the retarding voltage, applied between the scattering chamber and hemisphere, was 468.79 volts, such that electrons losing 21.21 eV in the scattering chamber, therefore, arrived at the W_3 with 10 eV energy and were transmitted to the multiplier. This procedure always provided a sufficiently high count rate (electrons hitting the multiplier) to allow the voltages of the two and three element electron lenses prior to the hemisphere to be optimised for maximum count rate.

After the beam was optimised,the incident beam energy could be changed with only L_4 being re-focussed since all other energies in the analyser section remain constant (see section 3.4.3).

As described earlier, the energy loss spectrum is obtained by scanning the voltage on L_4 and L_5, using a ramp generator. The ratemeter output and the ramp voltage generator were connected to the Y and X axes of a X-Y recorder.

Angular distribution (for a particular value of energy loss) were obtained by observing the variation of multiplier output (count rate) against the scattering angle.

Prior to the measurement of the angular distribtion for, say, the 21.21 eV energy loss peak in helium, values of count rate for conjugate positive and negative angles, within the range -7^{o} to $+7^{o}$ were measured to ensure symmetry of scattering about the mechanical zero angle of the spectrometer. The deflectors were used to achieve symmetry. The symmetry was checked before and after every angular distribution determination. Many sets of results were abandoned because of slight electron beam instability, causing non-symmetrical scattering.

CHAPTER 4

OBSERVATION OF THE OVERALL RESOLUTION OF THE MODIFIED SPECTROMETER

4.1 Introduction

The energy resolution, obtained after adapting the system, described previously (see Chapter 1), was high, approximately 1 eV compared with the expected 300 meV. Efforts to reduce this value and obtain energy loss spectra with better resolution, revealed the energy spread to be a function of the electron gun configuration.

In order to investigate the effect of different electron gun operating configurations on the overall resolution of the spectrometer, and the reason for such poor resolution, a series of experiments were carried out.

The literature suggests many different reasons for such anomalous energy spread in the electron gun. A brief outline of previous work is given in the next section, followed by the technique and results of our investigations.

4.2 Previous Work on Thermionic Emission

In order to free electrons from a cathode, energy must be imparted to them in their bound states to overcome their binding energy. If this energy is in form of heat, then "Thermionic Emission" occurs.

Fundamental theory predicts that the dependence of current and energy distribution, resulting from thermionic emission is as following:

$$J(E) = E\, e^{\frac{-E}{KT}} \tag{4.1}$$

where E is energy (ev), T is the cathode temperature (^{o}K) and K is the Boltzman Constant ($\frac{1}{11600}\ \frac{eV}{^{o}K}$).

There have been few investigations in the field of thermionic emission, particularly regarding the relationship between current density and energy distribution of the emitted electrons. The case of space-charge limited emission has been treated by Ivy (1954) who observed the energy distribution from a tungsten cathode, at a temperature characteristic of the cathode, to be Maxwellian. Boersch (1954) with an electron beam of energy 30 KeV, demonstrated a variation in energy distribution as a function of beam current and concluded that over a limited range of beam current densities, the energy half width (ΔE) depended linearly on the current density. A further series of measurement, however, revealed ΔE a function of $J^{\frac{1}{2}}$, a result not consistent with that of Dietrich. Dietrich (1956) concluded that energy distribution is a function of $J^{1/3}$ ($\Delta E \sim J^{1/3}$). Ulmer and his co-workers (1964) came to the conclusion that the dependency of energy distribution on current density is:

$$\Delta E \sim J^{1/3}\, E^{-\frac{1}{6}}\, \Delta E. \tag{4.2}$$

Simpson and Kuyatt (1966) found a range of different values for n in the equation $\Delta E \sim J^{n}$. The values they obtained for n were mostly 1, 1/3 and $\frac{1}{2}$. The energy dependence, despite what had been suggested earlier ($\Delta E \sim E^{-1/6}$), was concluded to be - 3/2. Thus, the energy spread equation which they presented was:

$$\Delta E = \Delta E_K + 1.4 \times 10^{-3} \frac{J}{E^{3/2}} \qquad (4.3)$$

where ΔE_K is F.W.H.M. of the cathode, and E is the energy of the beam.

4.3 Method of Studying the Resolution

The elastic scattering peak in molecular hydrogen or helium was chosen for this series of experiment. It was chosen since it is separated from the first inelastic peak in both hydrogen and helium by over 10 eV and may, therefore, be studied without interference from other transitions.

Investigations were carried out at 5^{o} scattering angle since measurements at scattering angles below 5^{o} and particularly at zero produced high count rates, and possible non-linearties in the multiplier output. The spectrometer was operated as described earlier. The variation in resolution with respect to variation of gun configuration was studied by measuring the energy half width of the elastically scattered electrons, recorded on the X-Y recorder.

4.4 Results

The variation of energy half width as a function of various electron currents, measured in the electron gun, for anode potentials 400 eV and 250 ev is presented in diagrams (4.1) and(4.2).

The total current, the current emerging from the anode, is the sum of the currents to A_2,A_3,L_1,L_2,W_1 and W_2; generally, the current to A_2 and L_1 was negligible. An increase of bias voltage for different A_1 voltages in these two diagrams, increases the beam current through A_1 until a plateau region is reached at a certain bias voltage. It is noticeable that the resolution also reaches a plateau region at the same value of bias voltage. These two diagrams confirm the dependence of the resolution on the electron current emerging from A_1:

$$\Delta E \sim I^n$$

The decrease of total current in diagram (4.1) at high bias voltages, is probably due to the bad focussing of electron beam in this region. Since the current hitting L_1 could not be monitored, it is possible that current could be 'lost' to this electrode under poor focussing conditions. The continued increase of $A_1(I)$ with bias voltage after the resolution has reached the plateau region (see diagrams (4.1) and (4.2)) indicates that the resolution is not a function of the current which is emitted from the cathode but is a function of the current which gets through the anode (total I).

Diagram (4.3) illustrates the resolution for different anode extraction energies. All have a minimum resolution of 270 meV, whereas their maxima are at 500, 550, 750 and 1100 meV for anode extraction energies of 100,150, 250 and 400 V respectively. The common minimum resolution was that expected from the spectrometer due to thermal energy spread of the thermionically produced electrons.

The variation of the resolution together with A_3 current, at a constant bias voltage (+ 20 eV) is plotted in diagram (4.4) as a function of the anode voltage and therefore represents a plot of the maximum resolution

attained at each anode voltage. It can be seen that, again, both curves are changing in the same direction, which is confirmation of the equation $\Delta E \sim J^n$.

However, variation of the anode and bias to produce the data in diagrams (4.1) to (4.4) necessarily required the variation of A_2,A_3 and A_4 potentials to maintain the focussed beam into the scattering chamber. The literature suggests (see previous section) a possible dependence of resolution on electron beam potential in the gun. To investigate this effect, the potential of A_2 was varied. The electron current passing through A_2 was kept constant (bias and A_1 potentials unaltered) and the potential of A_2 was varied whilst observing the overall resolution. It is seen in diagram (4.5) that the resolution for different values of A_2 voltage is more or less constant. It is concluded from this, that, the A_2 voltage has no significant effect on resolution.

Further, various other configurations of the electron gun (excepting bias and anode) produced only very small variations of the energy resolutions, leading us to conclude that the extraction stage of the electron gun is responsible for the anomalous energy spread observed in the present work.

Having studied the effects of the focussing stage of the gun on the resolution of the spectrometer, now we come to investigate the effect that the extraction system may have. However, we would not expect to get the same results as Ivy (1954).

Ivy did not observe anomalous energy spread in experiments he performed using a tungsten cathode, whereas our series of experiments were performed using an oxide cathode.

The results of the experiment, illustrated in diagrams (4.1) to (4.5) establish that ΔE is a function of the current which is transmitted through the anode, and not a function of the current which is hitting the anode (see particularly diagram 4.2). Having established this, the next consideration was the question of what effect the energy near the cathode, if any, may

have on the resolution.

To investigate this, I_{total} was kept constant (22 μA.) for different anode and bias voltages. This was achieved by choosing an anode voltage and tuning the total current by varying the bias voltage. The resolution was measured for each different anode/bias setting for 22 μA total current in order to isolate the dependence of resolution on current through A_1 already established. The results are plotted in diagram (4.6).

As is seen, the larger the anode extraction voltage (upper scale) the lower the bias voltage (lower scale) required for a given total current, and indeed, negative voltages were required for the high anode voltages. The resolution was changed by different gun extraction configurations (different anode and bias voltages). Therefore, it may be concluded that resolution is dependent on the energy of the electrons within the extraction system.. However, the proportionality factor cannot be deduced since the potential distribution, resulting from a triode extraction system, particularly near the cathode where the electrons will have only low energies, is complex. Thus it can only be deduced from this work that $\Delta E \sim E^n$ where n may be positive or negative.

ANODE ENERGY 400 eV

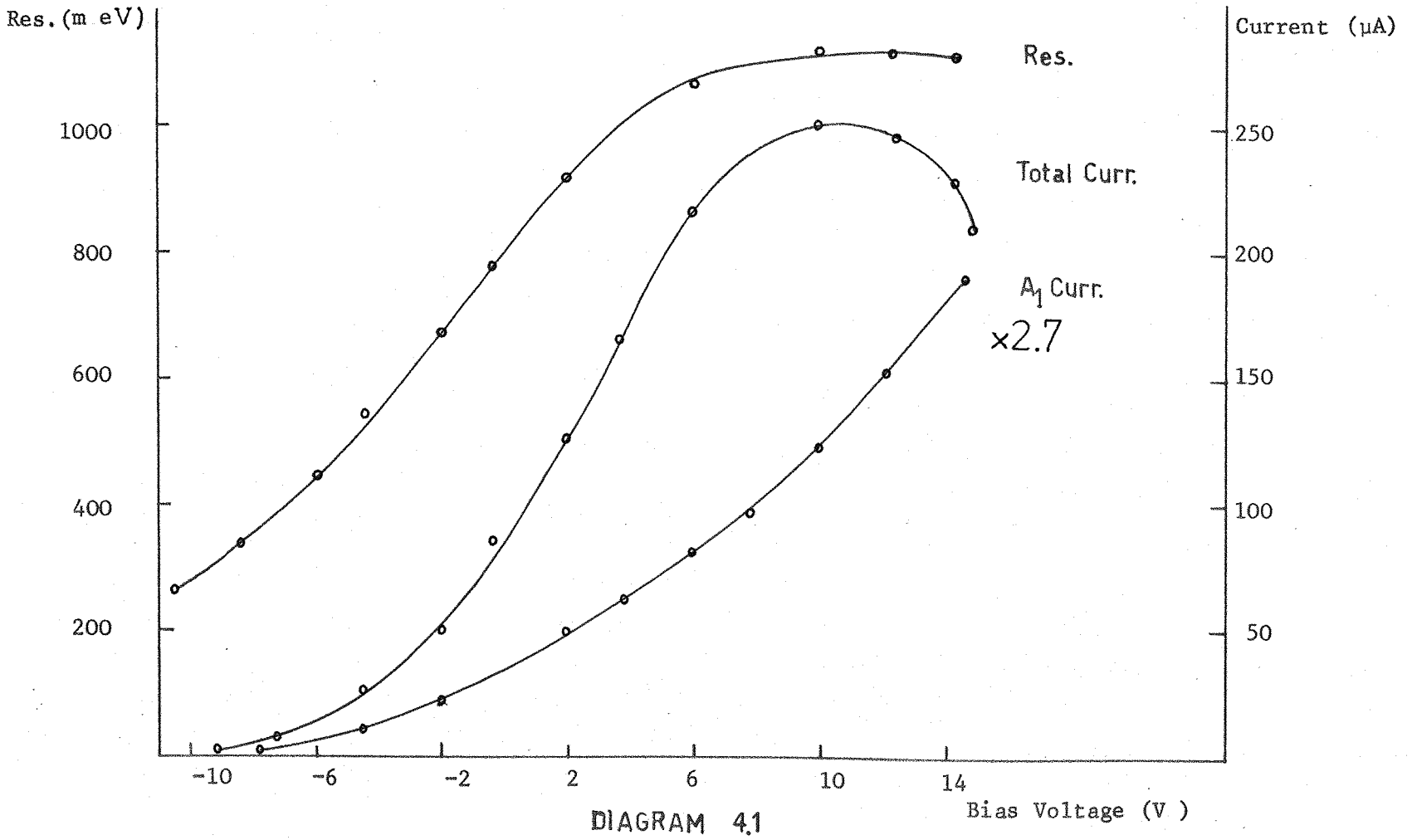

DIAGRAM 4.1

ANODE ENERGY 250 eV

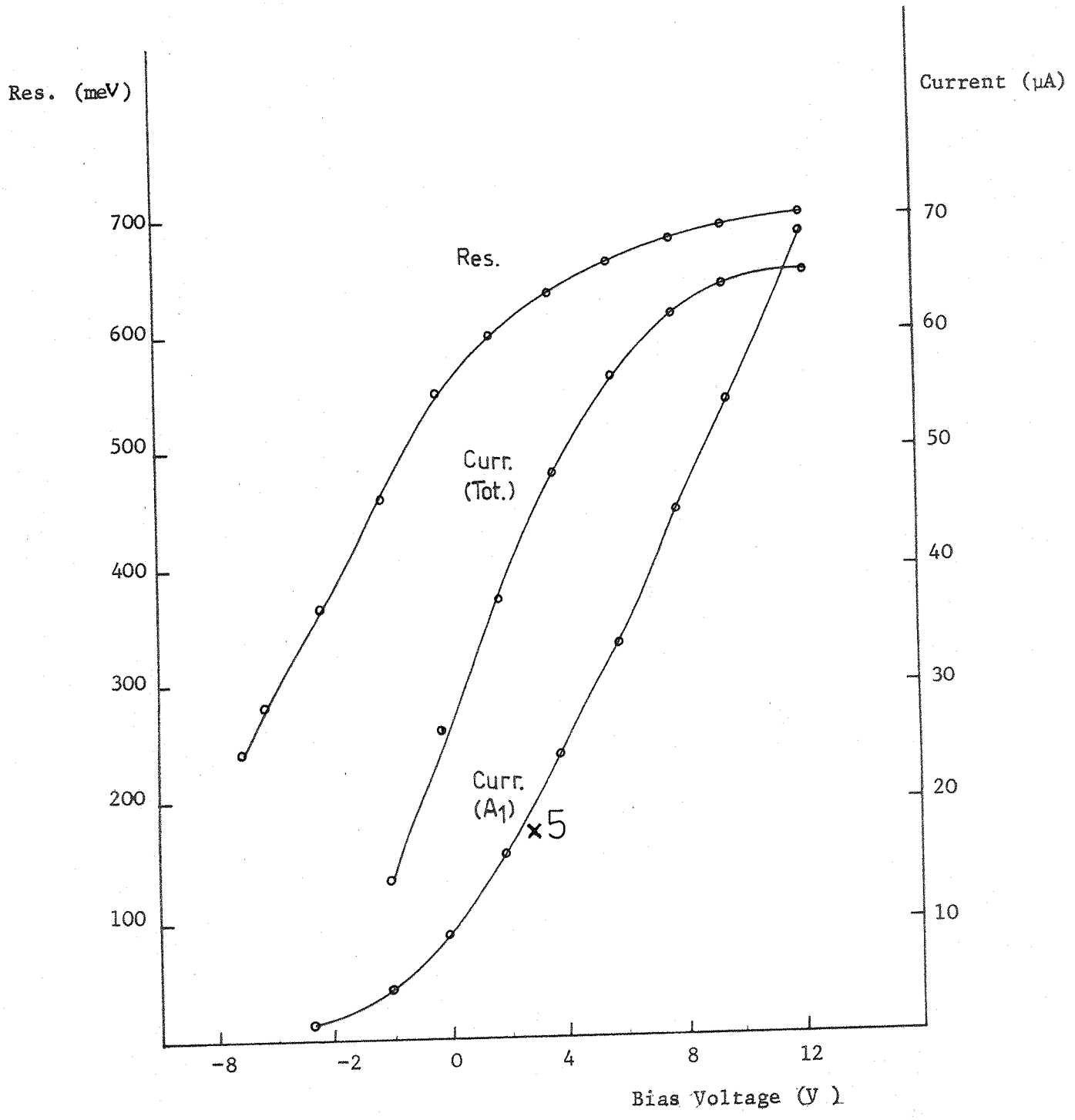

DIAGRAM 4.2

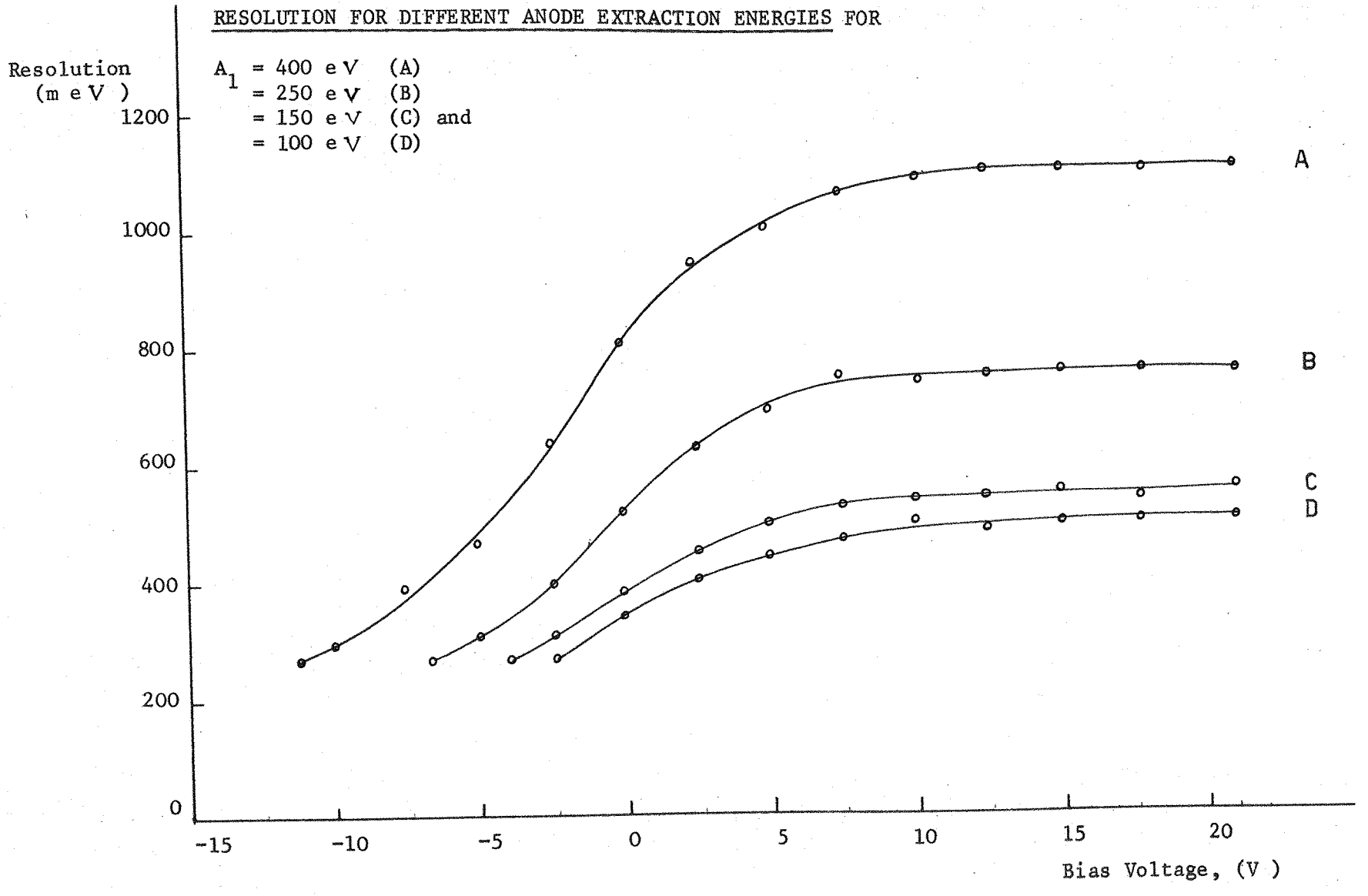
RESOLUTION FOR DIFFERENT ANODE EXTRACTION ENERGIES FOR
A1 = 400 eV (A)
= 250 eV (B)
= 150 eV (C) and
= 100 eV (D)
Resolution
(m eV)
1200
1000
800
600
400
200
0
-15
-10
-5
0
5
10
15
20
Bias Voltage, (V)
A
B
C
D

DIAGRAM 4.3

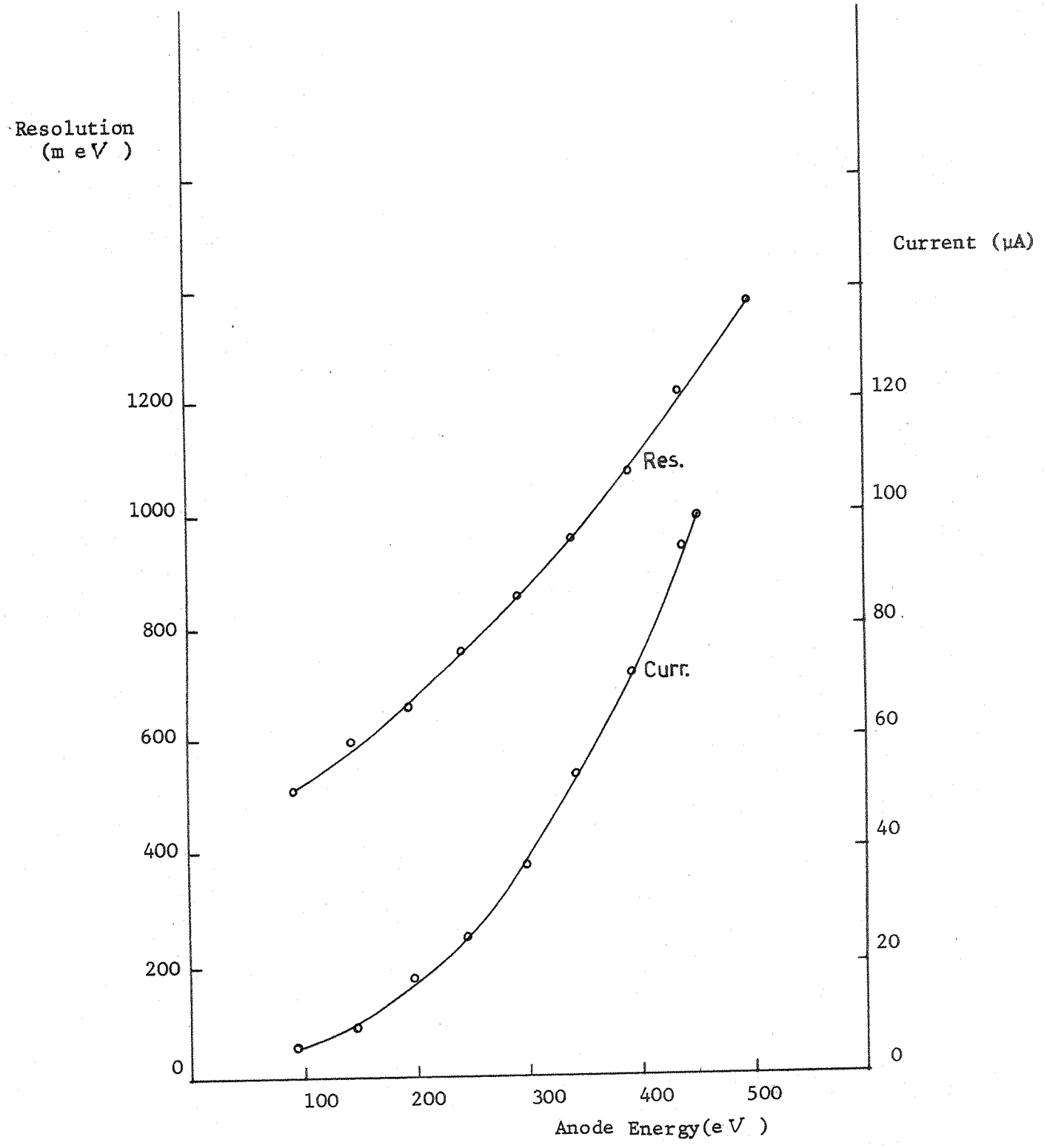
Resolution
(m eV)
Current (μA)
1200
1000
800
600
400
200
0
120
100
80
60
40
20
0
Res.
Curr.
100
200
300
400
500
Anode Energy(eV)

DIAGRAM 4.4

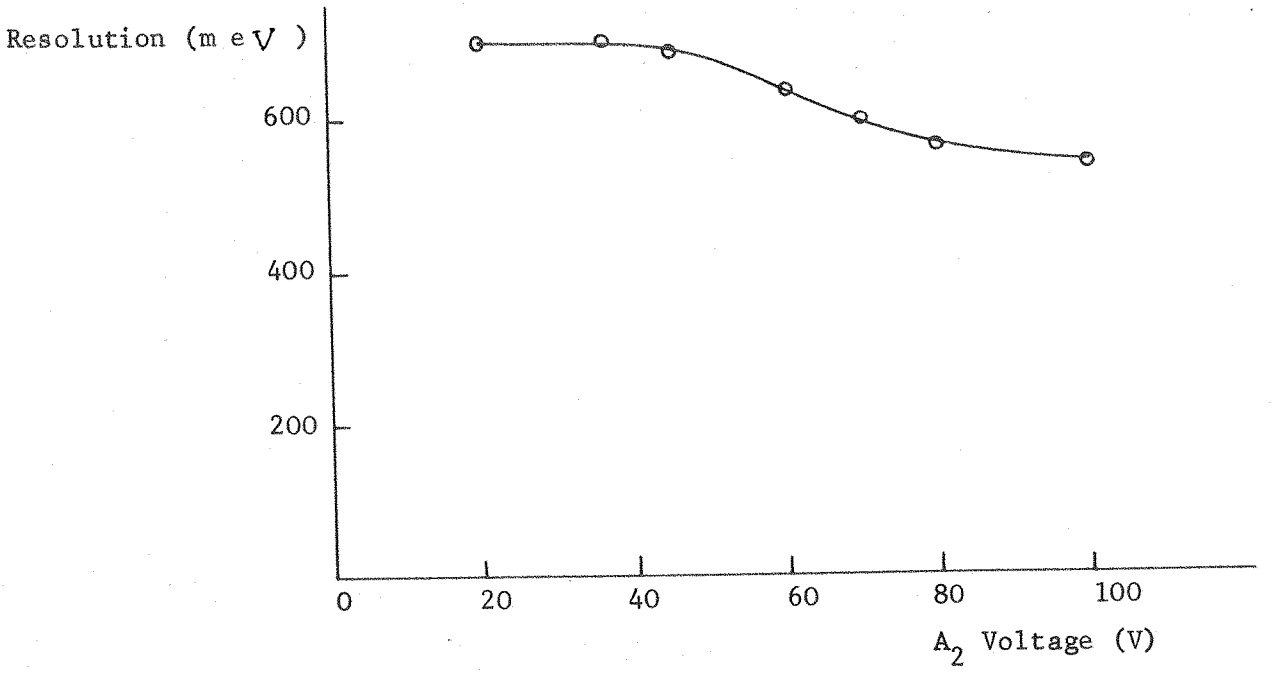

DIAGRAM 4.5

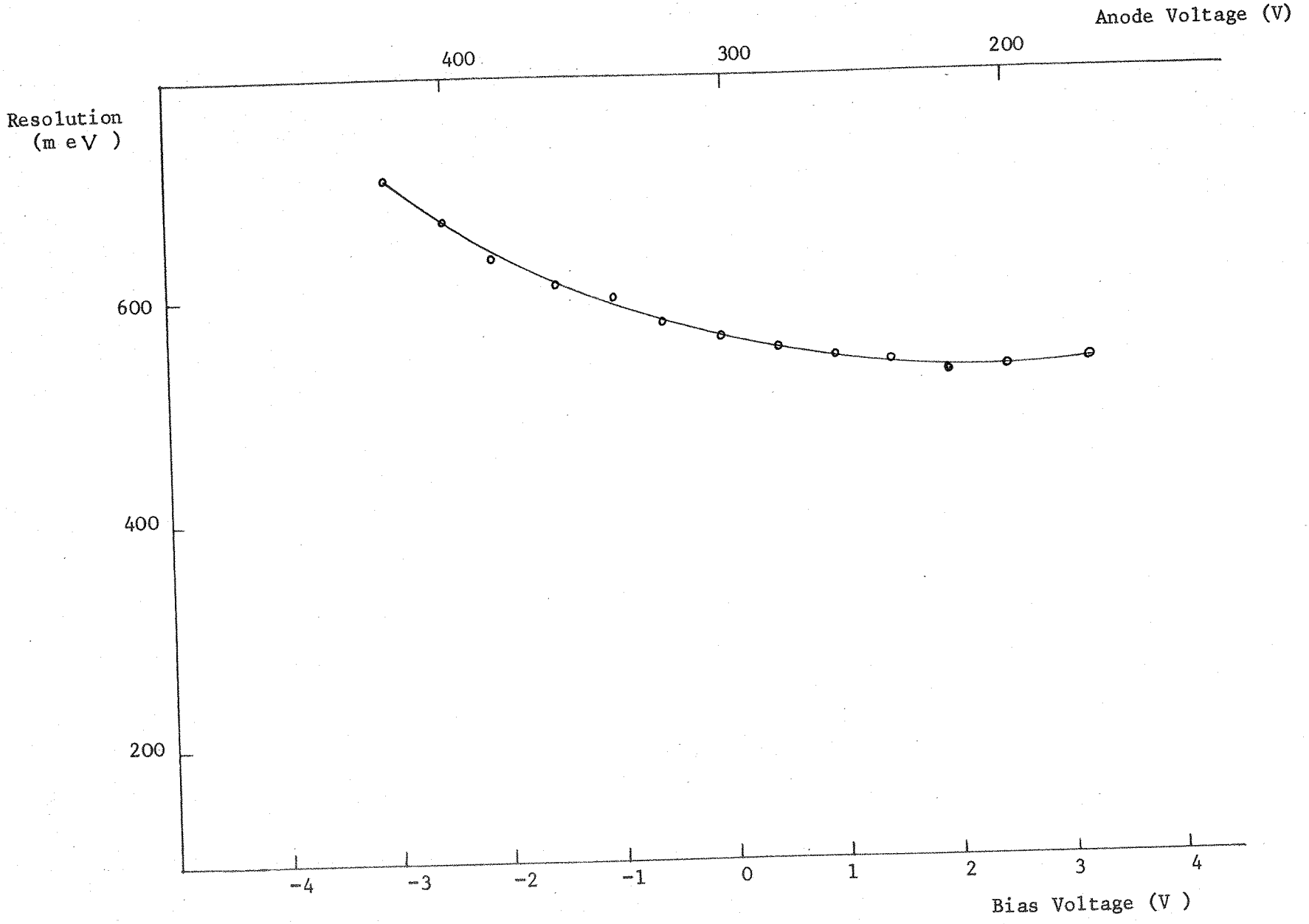
Anode Voltage (V)
400
300
200
Resolution
(m eV)
600
400
200
-4
-3
-2
-1
0
1
2
3
4
Bias Voltage (V)

DIAGRAM 4.6

4.5 Conclusion

This series of experiment enabled us to understand the parameters responsible for the anomalous energy spread within the incident electron beam of the spectrometer.

As a result of this, the spectrometer may now be operated with a resolution between 270 - 1000 meV. Unfortunately, it was not possible to establish the exact dependence of resolution on electron current and bias energy, but our results confirm earlier observations of the dependence of the resolution on these two factors.

CHAPTER 5

5.1 Results and Discussion

The high resolution energy-loss spectrum of the discharge afterglow of H_2 is shown in diagram (5.1). This spectrum was taken with the high resolution spectrometer (F.W.H.M. ≃ 80 mev) prior to modification. The spectrum clearly demonstrates the existence of atomic hydrogen, vibrationally excited H_2, and ground state H_2 in the afterglow. The transitions are also labelled in this diagram. A typical spectrum of the after-glow of H_2 with the modified low resolution spectrometer is shown in diagram 2. With the correct gun operation configuration (see section 3.3.3), the resolution is sufficiently good to resolve the atomic $1S \rightarrow (2S + 2p)$ transition from the molecular bands.

The scattered intensity of the $1S \rightarrow (2S + 2p)$ transition in atomic hydrogen, obtained from the electron energy-loss spectrometer, together, with the corresponding generalised oscillator strengths are presented in this section. The spectrometer configuration and the procedure for obtaining the results have previously been described in Chapter 3.

Attempts were made to prevent atom recombination in the region between discharge and scattering chamber, in order to have large values of electron-atom collision signal strengths. The glass tube was first coated with a thin layer of boric acid and then was baked in an oven at 200°C for five hours. This technique, however, was not particularly effective and the maximum atomic concentration in the discharge afterglow was found to be approximately 5%. A minimum of 10 watts microwave power was needed to maintain the discharge, while operation above 100 watts produced deterioration in the energy resolution of the spectrometer due to the increased length of the discharge afterglow extending into the electron beam interaction region. The relative increase in scattering intensity for the atomic transitions over this range of microwave power was only a factor of 2. The discharge

cavity to scattering chamber separation was 400 mm., this being the minimum distance set by the arrangement of the apparatus.

Angular calibration of the spectrometer was performed by comparing the results, obtained from the present apparatus for elastic electron-helium collision with those, experimentally obtained by Dillon and Lassettre (1975) and by Bromberg (1974). Table (5.1) shows the comparison. Within the combined experimental error of this comparison, our results show no detectable angular differences.

In the present experiment, the signal strengths were recorded at fixed incident electron energies as a function of various scattering angles. The condition of experiment are outlined in table (5.2). No pressure measurements were possible in the scattering chamber region and only an estimate is possible from consideration of gas flow condition and the measured gas inlet pressure.

The background pressure was generally used as a guide to the real scattering chamber pressure; no absolute value was required for data analysis. To ensure there is no error in results due to double scattering (see section 2.7), measurements were performed when the ratio of signal strengths at 7 degrees to 20 degrees showed no pressure dependence. To get to this state, the pressure was decreased until the ratio ($\frac{I_{7^o}}{I_{20^o}}$) remained constant. At high pressures (above 2×10^{-6} torr. background pressure), this ratio was found to become strongly pressure dependent. This established that the second term in equation (2.51) (see chapter 2), is significant at scattering chamber pressure corresponding to background pressure of 2×10^{-6}. The spectrometer was therefore operated with a background pressure of 5×10^{-7} torr. In this pressure region no pressure dependence of scattering ratios could be detected and it is concluded that within the experimental error of the results, the effect of the double scattering error may be neglected.

The experiment was performed for incident electrons with three different energies: 136, 200 and 300 eV and for scattering angles in the range 7 to

HIGH RESOLUTION ENERGY-LOSS SPECTRUM OF DISCHARGED HYDROGEN

(White, 1976)

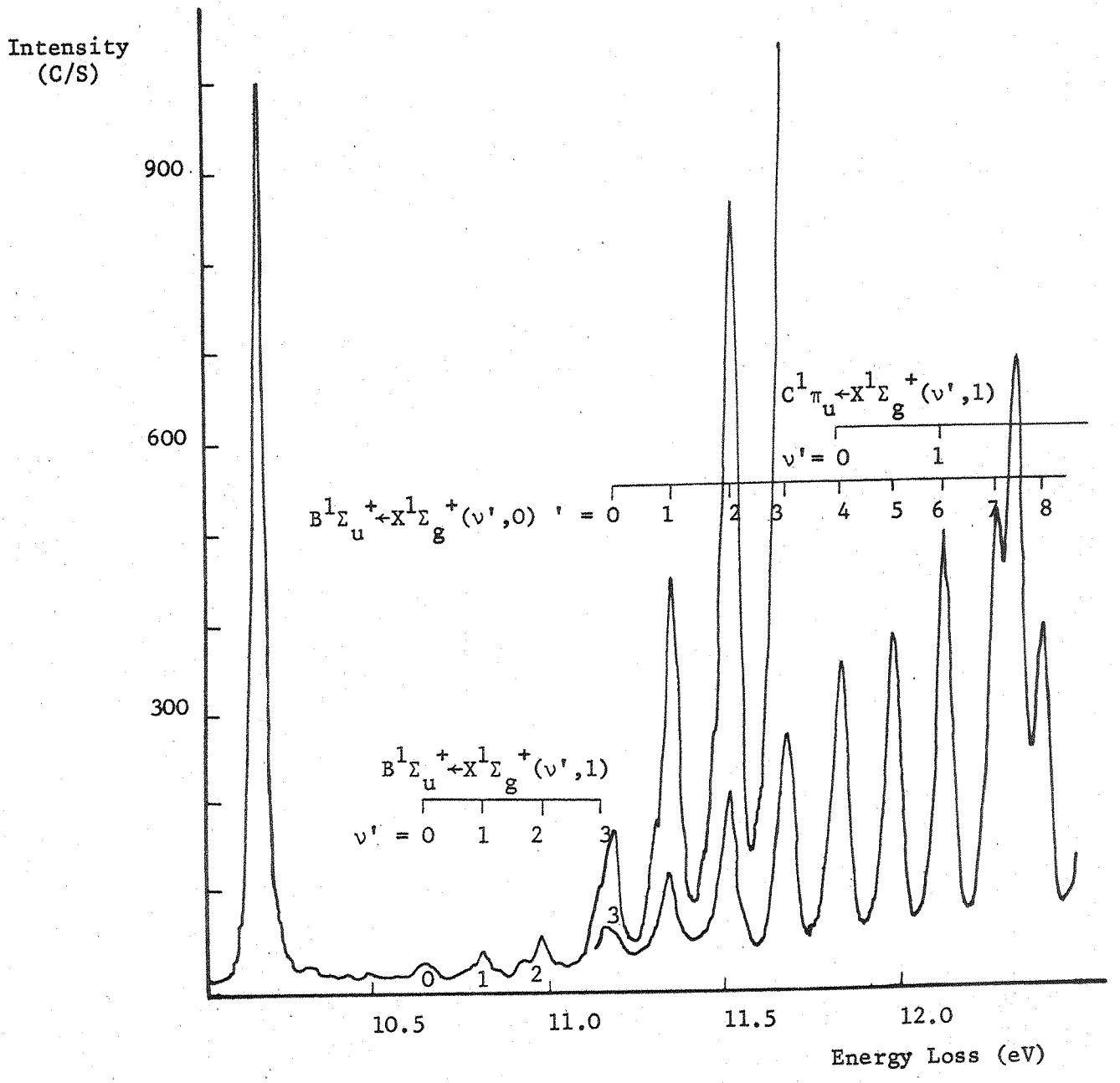

DIAGRAM 5.1

LOW RESOLUTION ENERGY LOSS SPECTRUM OF DISCHARGED HYDROGEN

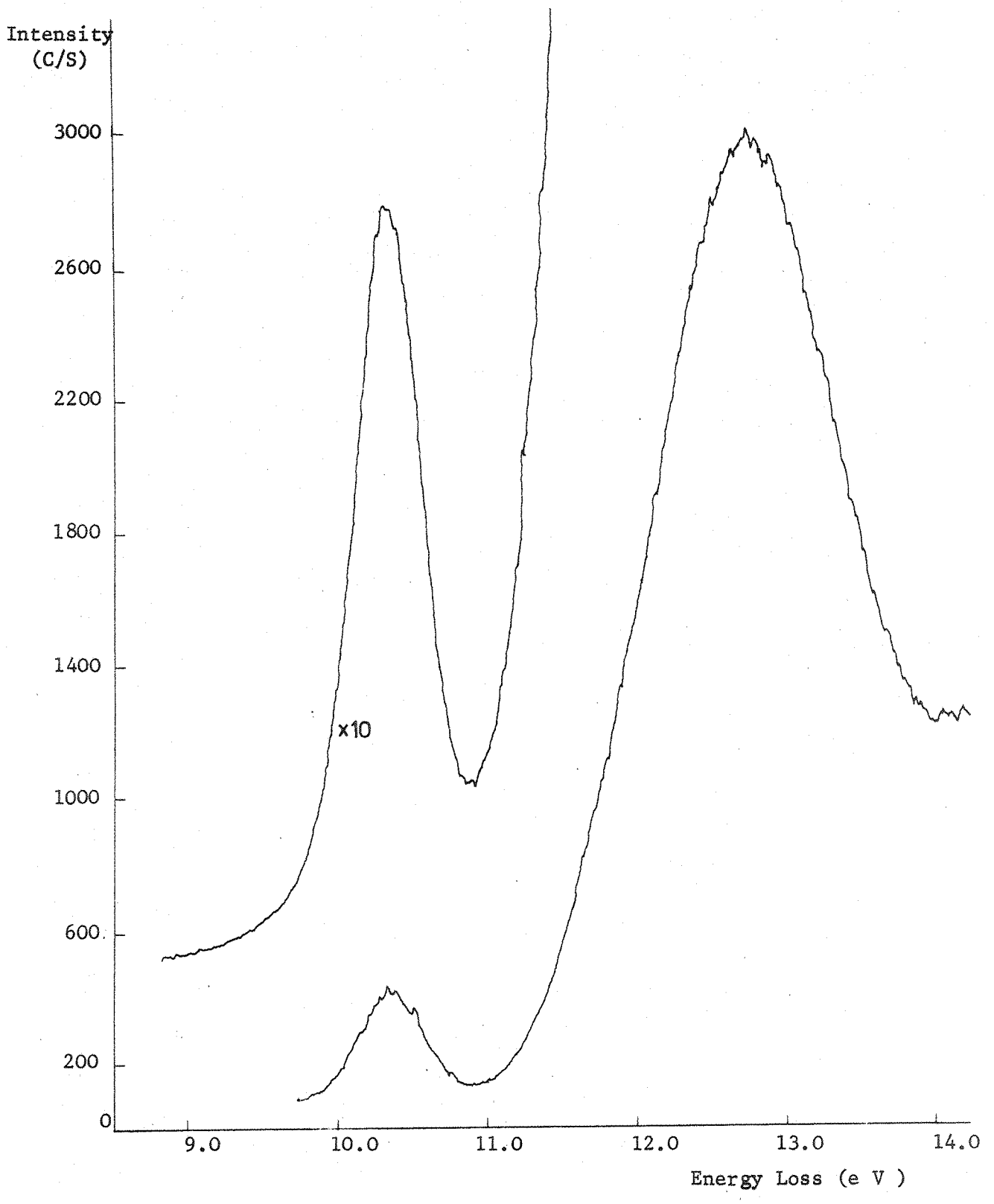

DIAGRAM 5.2

20 degrees. The reason for choosing these energies was to enable comparison of the results, from the present research, with those of Williams and Willis (1975).

The Generalised Oscillator Strength derived from the results of the present experiment for incident energies of 300 eV are shown in diagrams (5.3) and (5.4). In this work only relative values are obtained. In order to place these results on an absolute Generalised Oscillator Strength scale, normalisation to a known absolute value is required. This may be achieved by using a known experimental value, extrapolation to the optical Oscillator Strength at $(\Delta P)^2 = o$, or by using an accepted theoretical calculation. In this work the normalisation was performed, using theoretical data. The solid curves in diagrams 5.3 to 5.7 are the Born approximation.

In diagram (5.3) the normalisation was performed at $\theta = 7^o$, using the value predicted by the first Born approximation
Also shown in this diagram is the Born approximation for the region 7^o to 20^o, the Born approximation appears to give a good description of the scattering in this angular region.

However, it should be pointed out that most scattering theories follow the Born approximation closely in this angular region. diagram (5.4) illustrates this. The experimental data is now compared with the theoretical calculations of Kingston et al. (1976). The experimental data, normalised at 7^o to the calculation of Kingston et al. (1976) again agrees with that of theory within the experimental error. Unfortunately the small curve shape difference between the Born approximation and the Kingston et al. calculations are not resolvable within the experimental error.

We may only conclude, therefore, that the experimental data demonstrates a Born like behaviour in the range 7^o to 20^o for 300 eV scattering. The absolute values of the Generalised Oscillator Strength depend on the theoretical approximation, chosen for normalisation. The data of Kingston et al, and Born approximation never differ by more than 10% in the range

7^{o} to 20^{o}. In both diagrams (5.3) and (5.4) at 20^{o} the absolute value, obtained by Williams and Willis (1975) is plotted. For both normalisations (Kingston et al. and Born) the results of Williams et al. differs from the present work by 31% at 300 eV, 30% at 200 eV and 41% at 136 eV. This may indicate a systematic error in the results of Williams et al.

This conclusion is further supported by consideration of the optical Oscillator Strength. The experimental value of Generalised Oscillator Strength (0.4162) by Unsöld (1955) appears within 3% of that, predicted by the Born approximation.

If the data of Williams and Willis is used for the normalisation of the present experimental results, a most un-Born-like curve shape would be required in order to extrapolate our results from $(\Delta P)^2$ $\theta = 7^{o}$ to f_o at $(\Delta P)^2 = o$. As our experimental results show a Born-like behaviour in the region above $(\Delta P)^2$ $\theta = 7^{o}$ it is most unlikely that the region below $(\Delta P)^2$ $\theta = 7^{o}$ should exhibit non-Born-like behaviour since it is in this region that the Born approximation is most valid (i.e.: small $(\Delta P)^2$).

The above measurements were repeated for incident electron energies of 136 and 200 eV, the results of which are plotted out in diagrams (5.5) and (5.6). Again, within the experimental error, the data is in good agreement with the Born calculations. Also plotted in diagrams (5.5) and (5.6) are the absolute values determined by Williams et al (1975). Again large discrepancies are obvious. Since the Born approximation offers a good description of both the scattering in the region 7^{o} to 20^{o} and the optical oscillator strength it must be concluded that the data of Williams et al. is in error.

Diagram (5.7) contains all the Generalised Oscillator Strength measurements derived from the data, taken at 300, 200 and 136 eV incident electron energies together with the Born approximation curve. As previously discussed all agree, within the experimental error, with the Born approximation. Diagram (5.7) also demonstrates that the Generalised Oscillator Strength

for the 1S → (2S + 2p) transition of hydrogen show no incident energy dependence. This is a necessary condition for the validity of the Born approximation as discussed in section (2.2.1).

TABLE (5.1)

Signal strength of elastic electron-helium collision for 400 eV incident energy for scattering angles θ from 7^{o} to 20^{o}.

θ	Bromberg (1974)	Dillon & Lassettre (1975)	Present Work
7	1.877	1.794	1.850
8	1.493	1.448	1.511
9	1.212	1.170	1.220
10	1	1	1
12	0.698	0.724	0.691
14	0.506	0.516	0.512
16	0.377	0.369	0.379
18	0.282	0.280	0.280
20	0.213	0.217	0.228

TABLE (5.2)

Recording conditions for the results presented in this chapter.

Background Pressure (no gas flow)	5×10^{-7} torr
Background Pressure (with gas flow)	1×10^{-6} torr
Gas Line Pressure at inlet	about 200 m torr
Estimated Scattering Chamber Pressure	approximately 5 m torr
Detection mode	ratemeter
Ratemeter Time Constant	3.3 sec. for signal strengths higher than 100 C/S and 10 sec. for signal strengths lower than 100 C/S.
Cavity Input Power	100 watts
Cavity Reflected Power	zero

5.2 Error Sources

The following sources of error were considered in estimating the total error:

Statistical	<1%
Angular Resolution	3%
Energy Resolution	<1%
Multiple Scattering	<2%
Angular Callibration	≈2%
Channel Electron Multiplier Efficiency	≈2% (?)
Beam Fluctuation	<1%
Total R.M.S. error	5%

the mean value of the results shown in Figs. 3 - 7 are the average of many sets of results, taken over a period of several months. The error bars represent the errors (experimental and systematic) listed above.

GENERALISED OSCILLATOR STRENGTH AT 300 eV INCIDENT ENERGY

The absolute value at 20 degrees by Williams and Willis, (1975), in this diagram, and also in diagrams 5.4, 5.5, and 5.6, is indicated by ⊙.

Solid curves in these diagrams are the theoretical Born approximation data.

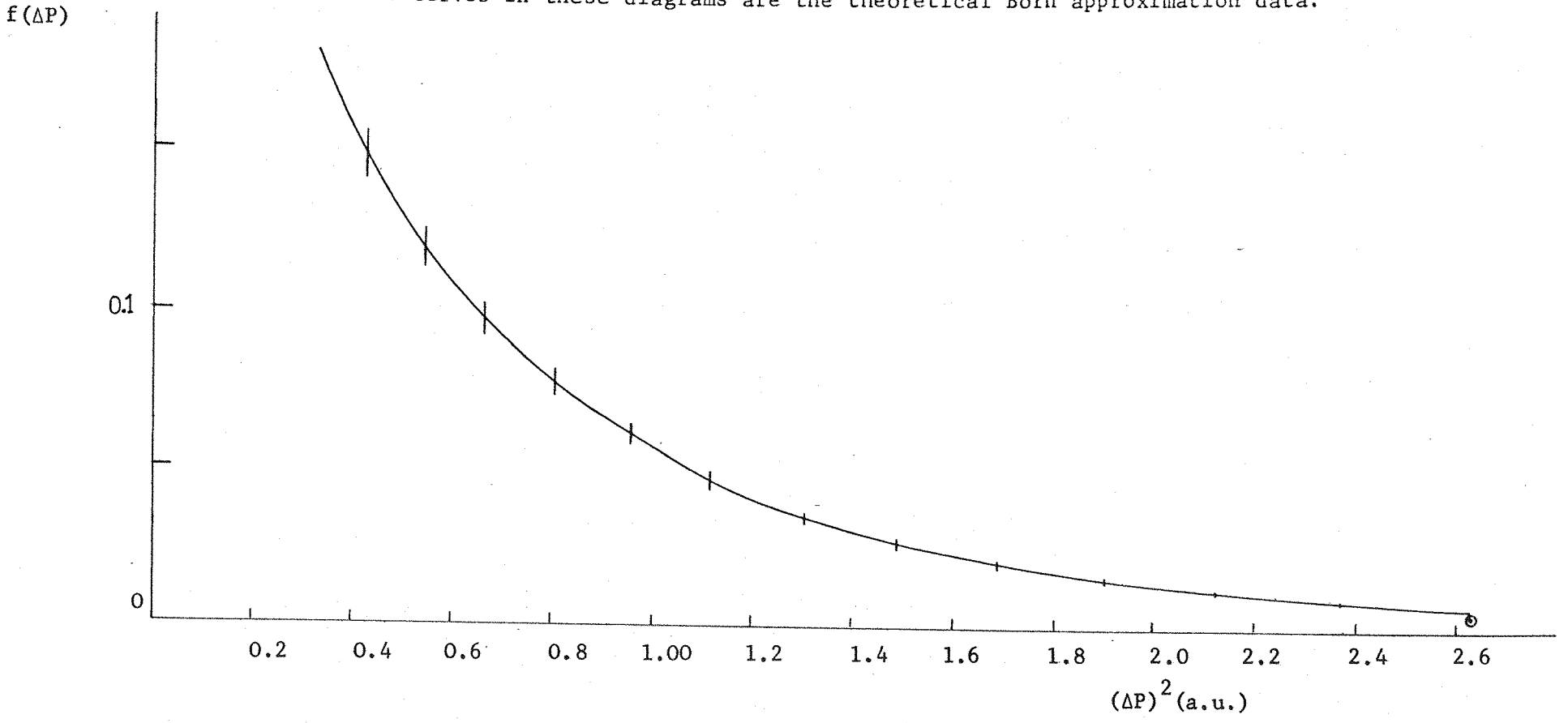

DIAGRAM 5.3

GENERALISED OSCILLATOR STRENGTH AT 300 eV INCIDENT ENERGY

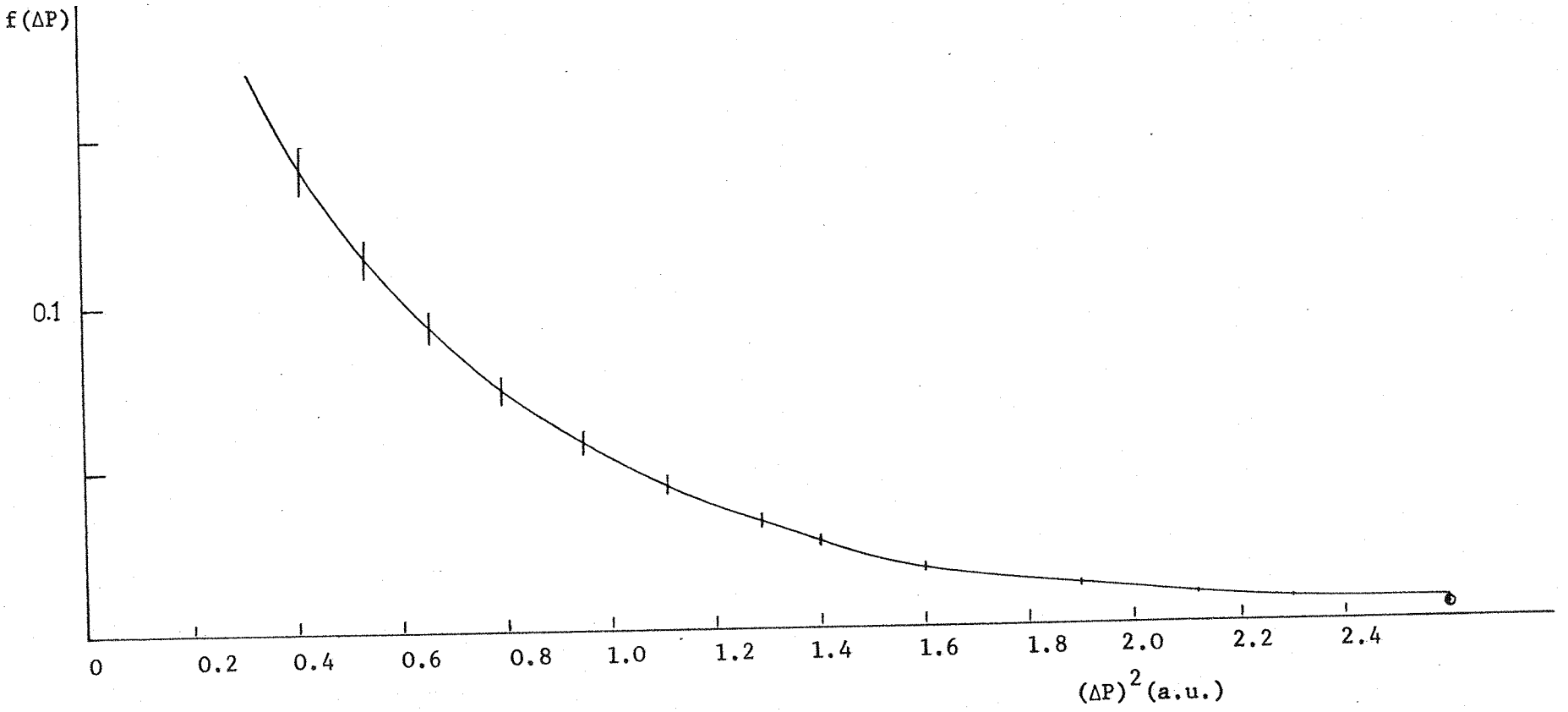

DIAGRAM 5.4

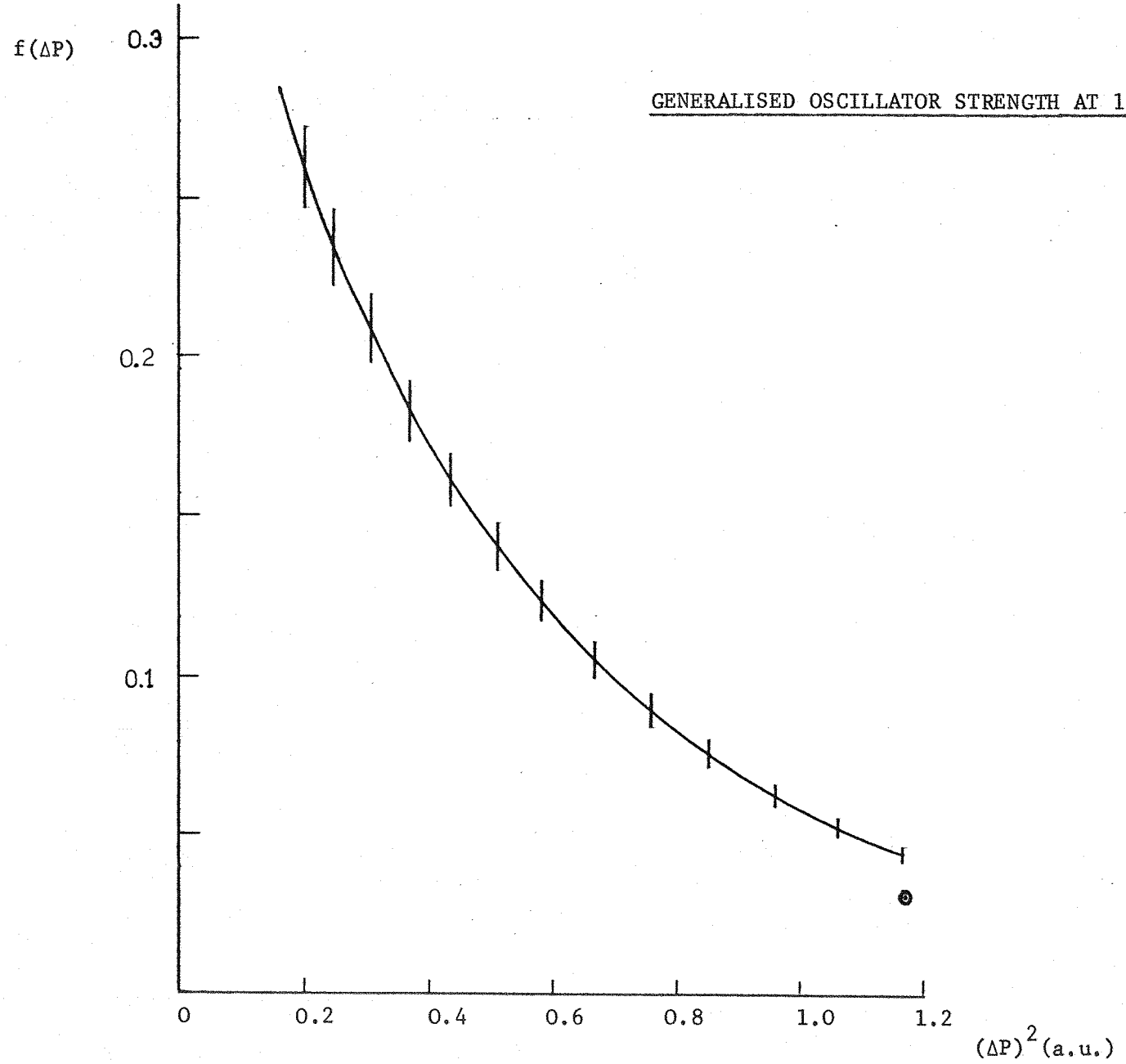

GENERALISED OSCILLATOR STRENGTH AT 136 eV INCIDENT ENERGY

DIAGRAM 5.5

GENERALISED OSCILLATOR STRENGTH AT 200 eV INCIDENT ENERGY

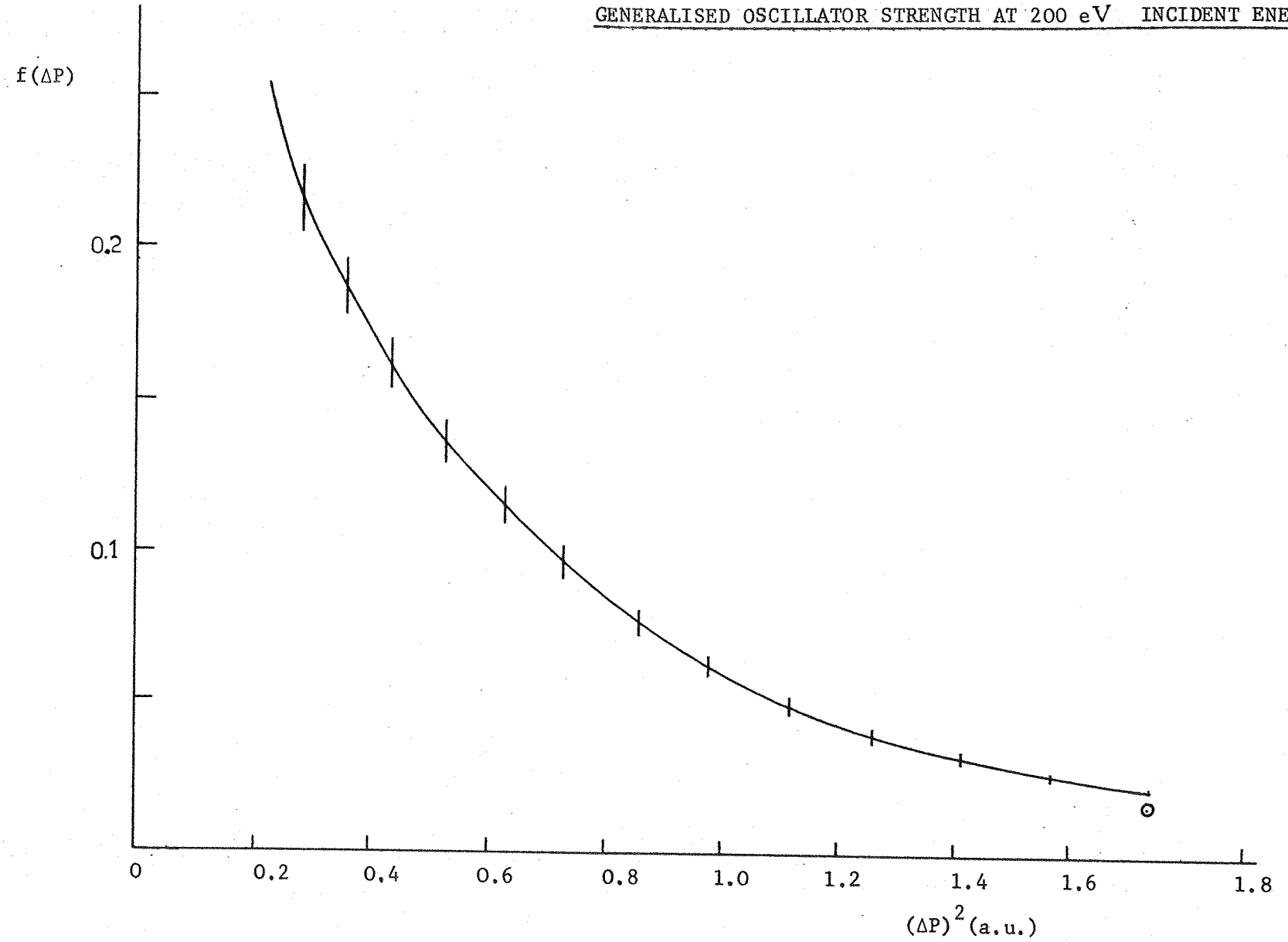

DIAGRAM 5.6

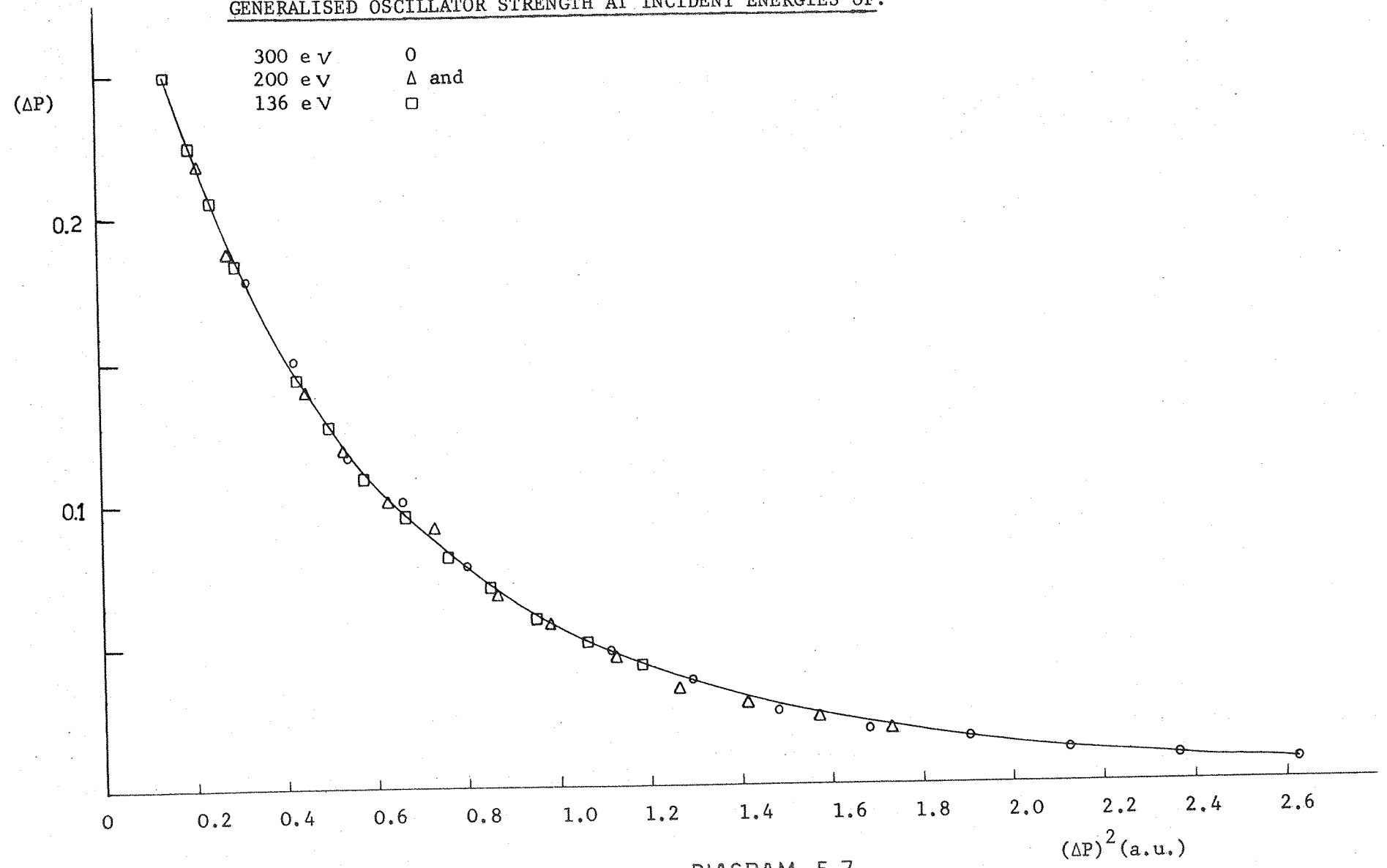
GENERALISED OSCILLATOR STRENGTH AT INCIDENT ENERGIES OF:
300 eV
200 eV
136 eV
0
Δ and
□
(ΔP)
0.2
0.1
0
0.2
0.4
0.6
0.8
1.0
1.2
1.4
1.6
1.8
2.0
2.2
2.4
2.6
(ΔP)² (a.u.)

DIAGRAM 5.7

REFERENCES

1. Altshuler S., (1952), Phys. Rev. 87, 992.
2. Aston F.W., (1919), Phil. Mag. 38, 710.
3. Bates D.R., and Damgaard A., (1949), Astrophys. J., 107, 383.
4. Bell K.L., Dose V., and Kingston A.E., (1969), J. Phys. B2, 831.
5. Bell K.L., Kennedy D.J., and Kingston A.E., (1968), J. Phys. B1, 204.
6. Bethe H., (1930), Ann. Physik 5, 325.
7. Blackstock A.W., Birkhoff R.D., and Slater M., (1955), Rev. Sci. Inst., 26, 274.
8. Boersch H., (1954), Z. Physik, 139, 115.
9. Bohr N., (1913), Phil. Mag. 25, 10.
10. Bromberg J.P., (1969), J. Chem. Phys. 50, 3906.
11. Bromberg J.P., (1974), J. Chem. Phys. 61, 963.
12. Bullard E.C., and Massey H.S.W., (1931), Proc. Roy. Soc. (London), A130, 579.
13. Burke P.G., Schey H.M., and Smith K., (1963), Phys. Rev. 129, 1258.
14. Chamberlain G.E., Simpson J.A., Mielczarek S.R., and Kuyatt C.E., (1967), J. Chem. Phys. 47, 4266.
15. Davydov A.S., (1965), "Quantum Mechanics", Pergamon Press Ltd.
16. Dietrich W., (1956), Z. Phys., 152, 306.
17. Dillon M.A. and Lassettre E.N., (1975), J. Chem. Phys. 62, 2373.
18. Doering J.P. and Williams A.J., (1967), J. Chem. Phys. 47, 4180.
19. Eckart C., (1930), Phys. Rev., 36, 878.
20. El-Sherbini Th.M. and Van Der Wiel M.J., (1972) Physica 59, 433.
21. Franck S. and Hertz G., (1919), Z. Phys. 20, 132.
22. Geiger J., (1964), Z. Phys. 177, 138.
23. Green L.C., Weber N.E. and Krawitz E., (1951) Astrophys. J., 113, 690.
24. Green T.A. and Peek J.M., (1968), Phys. Rev. 169, 37.
25. Harnwell G.P. (1929), Phys. Rev. 33, 559.
26. Harting E. and Read F.H., (1976), "Electrostatic Lenses", published by Elsevier.
27. Heddle D.W.O., (1969), J. Phys. E2, 1046.

28. Heddle D.W.O. and Kurepa M.V., (1970), J. Phys. E3, 552.

29. Hertell I.V., and Ross K.J., (1968), J. Phys. B: Atom. Molec. Phys., 1, 697.

30. Holt A.R., and Moiseivitsch B.L., (1968), J. Phys. B1, 36.

31. Hughes A.L. and Rojansky V., (1929), Phys. Rev. 34, 284.

32. Inokuti M. and Kim Y.K., (1968), Phys. Rev. 173, 154.

33. Ivy H.F., (1954), Advances in Electronics and Electron Physics, 6, 137.

34. Kim Y.K. and Inokuti M., (1968), Phys. Rev. 175, 176.

35. Kingston A.E., Fon W.C., and Burke P.G., (1976), J. Phys. B: Atom. Molec. Phys. 9, 605.

36. Klemperer O., and Barnett M.E., (1971), Electron Optics, 3rd ed., Cambridge University Press.

37. Kupperman A., Rice J.K., and Trajmar S., (1968), J. Phys. Chem. 72, 3894.

38. Kuyatt C.E., (1967), Private Text Communication.

39. Kuyatt C.E., and Simpson J.A., (1967), Rev. Sci. Inst. 38, 103.

40. Lassettre E.N. (1957), Ohio State Univ. Research Foundation, Scientific Report No. 1 (RF Project 464).

41. Lassettre E.N., and Jones E.A., (1964), J. Chem. Phys., 40, 1218.

42. Lassettre E.N., Krasnow M.E., and Silverman S., (1964), J. Chem. Phys. 40, 1242.

43. Lassettre E.N., and White E.R., (1958), Ohio State Univ. Research Foundation, Scientific Report No. 12.

44. Manson S.T., (1970), 6th International Conference on the Physics of Electronic and Atomic Collisions (abstracts), Cambridge, Mass., U.S.A. (M.I.T. Press), 626.

45. Massey H.S.W., (1956), "Handbuch der Physik", Springer-Verlag, Berlin.

46. Massey H.S.W., and Mohr C.B.O., (1931), Proc. Roy. Soc. (London) A132, 605.

47. Moiseiwitsch B.L., and Smith S.J., (1968), Rev. Mod. Phys. 40, 238.

48. Mott N.F. and Massey H.S.W., (1965), The Theory of Atomic Collision, 3rd ed., (Oxford University Press) [1949, 2nd ed.]

49. Möllenstedt G., (1949), Nachr. Wiss. Göttingen, 1, 83.

50. Newell W.R., Ross K.J., and Wickes J.B.P., (1971), J.Phys. B. 4, 684.

51. Oldham W.J.B., (1968), J. Phys. Rev. 166, 34.

52. Omidvar K., (1965), Phys. Rev., 140, A26.

53. Purcell E.M., (1938), Phys. Rev. 54, 818.

54. Rau A.R.P., and Fano U., (1967), Phys. Rev. 162, 68.

55. Read F.H., Adams A., and Soto-Montiel (1971), J.Phys. E4, 625.

56. Rothenstein W., (1954), Proc. Phys. Soc. (London) A67, 673.

57. Seaton M.J. (1951), Proc. Roy. Soc. (London) A208, 418.

58. Simpson J.A., (1964), Rev. Sci. Inst. 35, 1698.

59. Simpson J.A., and Kuyatt C.E., (1966), J. Appl. Phys. 37, 3805.

60. Simpson J.A., and Kuyatt C.E., (1963), Rev. Sci. Inst. 34, 265.

61. Soa E.A., (1959), Jena. Jb. 1, 115.

62. Spangenberg K., and Field L.M., (1943), Elec. Commun. 21, 194.

63. Trajmar S., Williams W., and Kuppermann A., (1971), J.Chem. Phys. 54, 2274.

64. Ulmer K., and Zimmermann B., (1964), Physik 182, 194.

65. Unsöld A., (1955), "Physik der Sternatmosphären", 2nd ed., Springer, Berlin.

66. Vander Wiel M.J., and Brion C.E., (1973), J. Elec. Spect. and Relat. Phenom., 1, 309.

67. Walske M.C., (1952), Phys. Rev. 88, 1283.

68. Walske M.C., (1956), Phys. Rev. 101, 940.

69. Whiddington R., and Priestley H., (1934), Proc. Roy. Soc. (London), A145, 462.

70. White M.D., and Ross K.J., (1976), J.Phys. B.: Atom. Molec. Phys. 9, 2147.

71. White M.D., (1976), Ph.D. Thesis, University of Southampton.

72. Williams J.F., and Willis B.A., (1975), J. Phys. B.: Atom. Molec. Phys., 8, 1641.

73. Womer R.L. (1934), Phys. Rev. 45, 689.